A STUDY OF INCLUSION BEHAVIOUR DURING ELECTROSLAG REMELTING

by

BRUNO C. BUREL

Ingénieur Civil des Mines

(Ecole Nationale Supérieure de la Métallurgie
et de l' Industrie des Mines, Nancy, FRANCE)

A THESIS SUBMITTED IN PARTIAL FULFILMENT OF
THE REQUIREMENTS FOR THE DEGREE OF
MASTER OF APPLIED SCIENCE

in the Department
of
Metallurgy

We accept this thesis as conforming
to the required standard

THE UNIVERSITY OF BRITISH COLUMBIA

JUNE, 1969

In presenting this thesis in partial fulfilment of the requirements for an advanced degree at the University of British Columbia, I agree that the Library shall make it freely available for reference and Study. I further agree that permission for extensive copying of this thesis for scholarly purposes may be granted by the Head of my Department or by his representatives. It is understood that copying or publication of this thesis for financial gain shall not be allowed without my written permission.

Department of Metallurgy

The University of British Columbia
Vancouver 8, Canada

Date September 15, 1969

"The cleanliness of steel, like beauty is very much in the eye of the beholder."

Melford 1962

ABSTRACT

Different mechanisms are proposed in the literature to describe the formation and behaviour of inclusions during electroslag remelting:

- dissolution in the liquid metal of the inclusions already present in the electrode and then renucleation in the freezing ingot.
- total or partial dissolution in the slag.
- exchange reactions between inclusions in the metal and the slag.
- entrapment in the freezing ingot of pieces of slag skin or droplets of slag.

The mechanism of dissolution of alumina inclusions in a 70/30 CaF_2/Al_2O_3 slag has been studied in detail. For this a new equilibrium diagram for the system CaF_2 - Al_2O_3 has been proposed and the diffusion coefficient of alumina in the slag has been determined by the rotating disk system. In a 70/30 CaF_2/Al_2O_3 slag at 1518°C the diffusion coefficient was estimated as $D = 8.5\ 10^{-9} m^2\ sec^{-1}$.

Calculations of the extent of the dissolution of alumina particles in the slag predicted that big particles (800 μ) might dissolve only partially in the slag. Particles of this size were introduced artificially in electrodes, but after elec-

troslag remelting a much larger number of relatively small (15 μ max) alumina, iron aluminates and iron oxide inclusions were found in the ingot. The same types of inclusions could also be observed in ingots obtained after remelting a Ferro Vac-E electrode. The presence of these inclusions cannot be explained by one the mechanisms proposed precedently (dissolution in the liquid metal and then renucleation or partial dissolution in the slag), but only by an electrolytic oxidation and electrolytic aluminum dissolution on the electrodes and then nucleation of deoxidation products in the freezing ingot.

ACKNOWLEDGEMENTS

The author wishes to express his gratitude to Dr. A. Mitchell for his continued interest and guidance throughout the period of study. Thanks are also extended to members of faculty and fellow graduate students for helpful discussions, and to the technical staff for their assistance with practical aspects of the work.

Financial assistance from Canada Council is gratefully acknowledged.

TABLE OF CONTENTS

Chapter		Page
General	Introduction	1
I	Inclusions	2
	1) influence of inclusions on the physical properties of steel	2
	2) problems in assessing inclusions	4
	3) formation growth and behaviour of inclusions during refining	7
	4) a modern method of improving metal quality: the electroslag remelting process	9
II	Scope of the Work: Behaviour of Inclusions During Electroslag Remelting	11
	Scope of this work	17
III	Determination of the Diffusion Coefficient . .	20
	1) mechanism of diffusion in molten salts . .	20
	2) methods of determination of diffusion coefficients in slags	22
	3) the rotating disk system	24
	4) practical applications of the rotating disk system for the determination of diffusion coefficients	25
IV	Thermodynamics of the System CaF_2 -Al_2O_3	27
	1) stability of the CaF_2 -Al_2O_3 mixture . . .	27
	2) equilibrium diagram for the system CaF_2 - Al_2O_3	30
V	Experimental Determination of the Diffusion Coefficient	35
	1) description of the apparatus	35
	2) preparation of the disks	37
	3) experimental procedure	37
	4) results	38
	5) discussion of the results	43

Chapter Page

a) accuracy of the measurements 43
b) error of calculation of the diffusion coefficient 46
c) discussion of the mechanism 48

VI Dissolution of Inclusions During Electroslag Remelting 50

1) Dissolution of a sphere 50
2) Dissolution, assuming similar flow conditions, to the rotating disk system 53

VII Experiments With Artificially Introduced Particles in the Electrode 56

1) The making of the electrodes 56
2) The melting conditions of the electrodes . 57
3) The remelting of the mild steel electrodes 57
a) inclusions in the electrode 57
b) inclusions in the ingot 58
4) The remelting of a Ferro Vac-E electrode . 64
a) the electrode 64
b) inclusions in the ingot 68
5) Electrochemical mechanism during remelting 73
6) Remarks on the solidification of the ingot. 74
a) solidification rate 74
b) concavity of the interface 75
c) interdendritic spacing 75

Conclusions 80

Suggestions for Future Work 82

References 84

Appendix I 87

Appendix II 88

Appendix III 89

Appendix IV 90

Appendix V 91

LIST OF TABLES

Table		Page
1	Diffusion coefficients of oxides in molten oxide mixtures	23
2	Determination of the diffusion coefficient of alumina in CaF_2 - Al_2O_3 slags	
3	Average solidification rate	74

LIST OF FIGURES

Number		Page
1	Schematic diagram of electroslag remelting	12
2	Inclusion removal as a function of the velocity of solidification determined from Stokes' law	18
3	CaF_2 - Al_2O_3 binary diagram determined in this work	32
4	Comparison of the CaF_2 - Al_2O_3 binary diagram determined in this work with other determinations	33
5	Schematic diagram of the rotating disk apparatus	36
6	Weight loss of the alumina disks versus the square root of the rotating speed in 70/30 CaF_2/Al_2O_3 slag at 1518°C	40
7	Weight loss of the alumina disks versus the square root of the rotating speed in 70/30 CaF_2/Al_2O_3 slag at 1509°C	41
8	Weight loss of the alumina disks versus the square root of the rotating speed in 80/20 CaF_2/Al_2O_3 slag at 1500°C	42
9	Typical inclusion in the mild steel electrode (X 1200)	59
10	X-Ray picture for Ca (X 1200)	60
11	X-Ray picture for Mn (X 1200)	61
12	X-Ray picture for Si (x 1200)	62
13	Absorbed electron image plus S trace	63
14	Typical inclusion in the ingot after remelting of the mild steel electrode (X 1200)	65
15	X-Ray picture for Al (X 1200)	66

Number		Page
16	X-Ray picture for Mn (X 1200)	67
17	Cluster of inclusions in the ingot after remelting of a Ferro Vac-E electrode	70
18	X-Ray picture for Al (X 1200)	71
19	X-Ray picture for Fe (X 1200)	72
20	Etched section of the ingot after remelting the Ferro Vac-E electrode	76
21	Dendrites on the polished and etched surface of a specimen of the ingot obtained after remelting a mild steel electrode (X 8)	77

LIST OF SYMBOLS

a	activity
a_o	initial radius of a sphere
C	solute concentration
C_o	initial solute concentration
C_i	sphere solution concentration
C_s	concentration of solute in a sphere
C_{Sat}	solubility of the solute
ΔC	concentration gradient
$C\pm$	concentration of ions
d	slag density
d'	electrode diameter
D	diffusion coefficient
$D_\pm$	diffusion coefficient of the ions
D'	ingot diameter
D_i	self diffusion coefficient
F	Faraday's constant
ΔF	free energy change
g	gravity constant
i	interdendritic spacing
J	flux of solute
k	Boltzmann's constant
N	number of revolutions per minute
P	pressure
r	radius of a particle

R	radius of a disk
Re	Reynolds' number
t	time
T	absolute temperature
U	velocity of the liquid
v	rising velocity of a particle (Stokes' law)
V	solidification velocity
V_2	axial component of the liquid velocity
X	length of a cone exposed to liquid flow
Y	position of the interface
z_i	valence of an ion
α	ratio of the volume attributed to a mass of solute in the solution to the volume occupied by the same mass in the pure solute
β	parameter
δ	diffusion boundary layer
η	dynamic viscosity
Λ_i	equivalent ionic conductance
ν	kinematic viscosity
ρ_m	density of the metal
ρ_{incl}	density of an inclusion
σ	standard error
ω	angular velocity

GENERAL INTRODUCTION

High-strength, tough, heat resistant, ball-bearing, stainless, instrumental and precision steels and alloys are the basis of the development of new technologies. The requirements set for the various special properties of these materials are increasing sharply. So, new metallurgical processes have to be designed to produce metals possessing such properties. The electroslag remelting process is a new method of increasing the quality of metal, competing successfully with the other technological processes used in the steel industry, such as the vacuum arc remelting process.

In order to improve the performances of the electroslag remelting process, a better understanding of its metallurgical mechanisms is necessary. In particular, since most physical properties of steels and alloys are held to be related to the inclusion content of the metal, further knowledge on how inclusions behave during processing should lead to a better control of these properties in the product. The object of the present work is to provide more information on inclusion behaviour during electroslag remelting. It is first necessary to make of review of the tools needed, and to make a synthesis of all the mechanisms of formation and growth of inclusions, in order to build a model for their removal during electroslag remelting. The particular case of Al_2O_3 inclusions has been chosen to illustrate some of the mechanisms involved.

I. INCLUSIONS

The presence of heterogeneous non-metallic inclusions in steel affects the physical properties of this steel. This influence of inclusions is difficult to assess for the steel-maker and steel-user, because many interrelated factors are involved. However, only a better knowledge of their origin, and behaviour during refining can lead to improvements in the control of their content in the metal.

(1) Influence of Inclusions on the Physical Properties of Steel

Kiessling[1], in his book on inclusions describes present knowledge on the influence of inclusions on the physical properties of steels.

The relationship between these properties and the non-metallic content of steel is governed by many factors [1,2]

- the shape of the inclusions
- their size
- their physical and chemical properties
- their distribution and orientation with reference to the applied stress
- the physical properties of the parent metal and the relative modification of those properties in the vicinity of the inclusions.

Kiessling[1] points out the importance of the index of deformability which gives a measurement of the relative plasticity

of the steel and the inclusions.

Inclusions are not always detrimental to steel properties. Thus, MnS inclusions are considered to be of advantage for the machinability of the steel, because they act as stress-raisers in the region of the shear-plane of the swarf. Their shape and size is of great importance. The larger globular MnS inclusions deform plastically (during machining), along shear planes of the swarf to some elongated stress-raising plates, whereas the smaller ones become so thin that their stress-raising effect becomes negligible.

The influence of inclusions on the fatigue properties of steel has been studied for high-strength and ball-bearing steels (A.I.S.I. specification 52100 C 1%, Cr 1.5%). Inclusions of low index of deformability such as calcium aluminates and Al_2O_3 inclusions (index of deformability $\nu=0$) are most detrimental. Cavities develop around calcium aluminates, increase the tensile stress in their immediate vicinity and initiate cracks[1,2]. Sharp edged Al_2O_3 inclusions are also the nuclei of cracks.

Duckworth and Ineson[3] have studied the influence of inclusion size and position on the fatigue life of ball bearing steel. Surface inclusions of any size, provided they are of the type which impairs fatigue strength, are deleterious. With failure which originates just below the surface, the size below which no effect on fatigue is observed is 10 μ. Deeper below

the skin, only large inclusions can cause failure.

Inclusions have also a significant effect on other physical properties of steels such as hot-shortness, which is the tendency to brittle fracture in the hot-forming range, surface finish, weldability, hot-tearing, etc.

The effect of inclusions with a diameter less than 1 μ has been much less studied. However according to Kiessling[1] 98% of all oxide inclusions are smaller than 0.2 μ, although they represent only 1 to 2% of the total oxygen in steel. They may act as nuclei for precipitation of other phases, such as carbides and influence grain-growth and grain-boundary movement. Many physical properties may therefore be indirectly related to these non-metallic inclusions, visible only with electron microscope.

(2) Problems of Assessing Inclusions

Numerous factors and complex mechanisms interplay to modify the physical properties of the steel. From the steel-maker and steel-user point of view, the question is to know whether or not a certain steel that has been produced will meet the requirements for which it has been designed.

Allmand[4] gives a complete review of methods for assessing non-metallic inclusions in steel, supposedly related to the physical properties of the steel. The two most widely used

methods are the Fox and Jernkontoret inclusion counts. The basis of these methods is a visual comparison of inclusions examined by microscope on a sample of metal with standard charts. The charts of the Fox count does not take into account the type of inclusions, whereas the Jernkontoret count differentiates between types of inclusion. Also, although its use is not as simple as that of the Fox count, the Jernkontoret count gives more information such as frequency curves for each type of inclusion. The main criticism of the two methods is that as comparison methods they are subject to personal judgement. None of these empirical methods is capable of providing all the information necessary in an ideal count for determining the relationship between inclusions and physical properties of steel. Thus, Atkinson[2] finds no relation between the Fox count and the fatigue properties of the samples that he has examined.

Kiessling[5] and Snow[6] give a complete review of the methods available to identify inclusions with the metallographic microscope. Inclusions can be extracted by different techniques.[7,8] The acid solution method is known to isolate oxides only, particularily Al_2O_3 and SiO_2. Other phases can be isolated by halogen solutions. The electrolytic method is perhaps the best. If a sample is electrolyzed below the decomposition potential of a phase, this phase is not decomposed. Anodic corrosion of the matrix occurs around non-attacked particles of this phase, which can thus be isolated.

The size distribution of inclusions can be measured by microscopic or sedimentation methods, but with these techniques the absolute number of particles contained in a unit volume of specimen cannot be determined. The particle size analyzer Coulter Counter described by Yoshio Muyashita and Katsuhiko Nistnkawa[9] is capable of giving this information. The particles are dispersed in an electrolyte in a beaker equipped with two electrodes. One of them is contained in a sealed glass tube having a small hole. The electrolyte is forced to flow from the beaker to the tube through the aperture. As a particle travels through the aperture, the cross-sectional area decreases and the corresponding increase in resistance gives a momentary drop in the current flow which is converted to a pulse. Accordingly, the number of particles and their size distribution can be determined from the number and the heights of the pulses. In summary, the industrial methods of assessing inclusions do not satisfactorily give a relationship with the physical properties of the steel. But the information necessary to build this relationship can be given by the methods of identification and measurement of the size and distribution of the particles. The industrial techniques of counting inclusions must be chosen to yield the appropriate information related to the particular physical properties expected from the steel.

(3) Formation, Growth and Behaviour of Inclusions During Refining

In order to make a steel of specified physical properties, it is important to control, as much as possible, the mechanisms of formation, growth and behaviour of these inclusions during refining of the steel.

Besides the eroded refractory particles and other pieces of dirt carried with the liquid stream into the mould, inclusions can be classified into two categories from the point of view of the mechanism of their formation:

- primary inclusions. These are reaction products formed in the melt, e.g. deoxidation products. Those which are not floated out of the liquid before solidification will will remain in the ingot.
- secondary inclusions are formed during cooling and solidification. They are oxide inclusions formed during freezing because of the low solubility of oxygen in δ - ferrite. They are also sulphides, nitrides and carbides which dissociate readily in liquid iron solutions.

Torsell[10], Turkdogan[11], Turpin and Elliott[12] have studied the mechanism of nucleation and growth of deoxidation products. Inclusions can form by homogeneous nucleation. In particular, Turpin and Elliott[12] have shown that variations in the deoxidizer or oxygen supersaturation concentrations lead to the

nucleation of different oxide phases. For instance, in the Fe-O-Al system homogeneous nucleation occurs with the formation of an iron aluminate low in Al_2O_3 below approximatively 0.01% Al. Above approximately 0.03% Al, Al_2O_3(s) is produced, and both of the above phases (and perhaps FeO Al_2O_3 (hercynite)), are formed in the intermediate range.

Torsell, Catellier and Olette[13] report however that the important supersaturation needed for homogeneous nucleation cannot be obtained experimentally and that the nucleation of inclusions can only be explained by a mechanism of heteregeneous nucleation.

Once they have attained the critical nucleus size, inclusions can grow by different mechanisms:

- by diffusion of oxygen or of the deoxidizer dissolved in the melt.
- by diffusional coalescence, i.e. by diffusion of oxygen from smaller inclusions which are not in equilibrium with their surroundings.
- by collisions due to different velocity of rise according to Stokes'law. Big inclusions moving faster may collide with smaller ones, break the iron film between them and coalesce.
- by collisions due to stirring which creates velocity gradients. Stirring increases the number of collisions, but is generally not large enough to break up a particle, as reported by Torsell.[10]

Secondary inclusions appear during solidification. Further deoxidation reactions occur during freezing as oxygen becomes less and less soluble in the iron[14]. The theory of nucleation applies also to the formation of oxide nuclei on solidification[12]. The solidification rate is an important factor influencing the removal of inclusions. It controls the interdendritic spacing[15]. Dendrites are solid projections ahead of the freezing interface. Inclusions may be trapped between two dendrites or pushed ahead of the freezing front, depending on their relative size with respect to the interdendritic spacing. Also, the advancing interface rejects solutes. The solute rich liquid may be trapped within the interdendritic cells, where the solute can precipitate as inclusions.

(4) A Modern Method of Increasing Metal Quality: The Electroslag Remelting Process

In order to produce steels of specially high physical properties, several methods are used, which in particular favour certain mechanisms that control inclusion formation, size and distribution. They aim at improving the quality of the liquid metal and the structure of the ingot. The electroslag remelting process,which is the object of the present work, is one of these methods and is already widely used. As in the vacuum arc remelting process, vertical solidification favours the removal of inclusions. Although there is a lesser reduction of the gaseous content than by vacuum arc remelting, the electroslag

remelting process gives steels and alloys of equivalent physical properties.[16]

The increased density and homogeneity of the metal, the reduction of its contamination by non-metallic inclusions and, most important, the uniform distribution of these inclusions, achieved as a result of electroslag remelting, are held to be responsible for a sharp reduction of the anisotropy of the mechanical properties of the steel. Also, the plasticity at normal, high and low temperatures is increased. The deformability of highly alloyed steels during hot mechanical working and the forgeability are improved because of the purity of the metal with respect to non-metallic inclusions and the absence of coarse, line accumulations of these inclusions. Also, the lifetime of bearings, particularily sensitive to inclusion content and distribution,[3] is substantially higher than that of bearings of the usual metal.[16,17,18]

II. SCOPE OF THIS WORK: BEHAVIOUR OF INCLUSIONS DURING ELECTROSLAG REMELTING

The present work is concerned with the behaviour of inclusions during electroslag remelting. Descriptions of the process are given in various papers[16,17,19]

A metal electrode is melted in a molten flux pool, contained in a water-cooled mold. High current at low voltage is delivered through the electrode to the flux. Joule heating of the flux enables it to melt, to remain at high temperature and to cause the melting of the electrode. Drops of molten metal form at the tip of the electrode. They go through the molten flux, are solidified and form the ingot (Figure 1). A thin skin of slag exists around the slag pool and the solidifying ingot. The structure of this layer, which influences the surface quality of the ingot, has been discussed by Mitchell and Etienne[20]. It is found to be dependent on the melting rate of the electrode and on the melting point of the slag.

The liquid metal is in contact with a slag and an important feature of the electroslag remelting process is that the metal presents a large surface to the slag throughout the operation, first as it flows along the tip of the electrode to form a drop, then as the drop goes through the slag and finally arrives at the slag/metal interface where it enters the metal molten pool above the solidifying ingot. Moreover, although this point has not yet been elucidated, it is to be believed that the variations

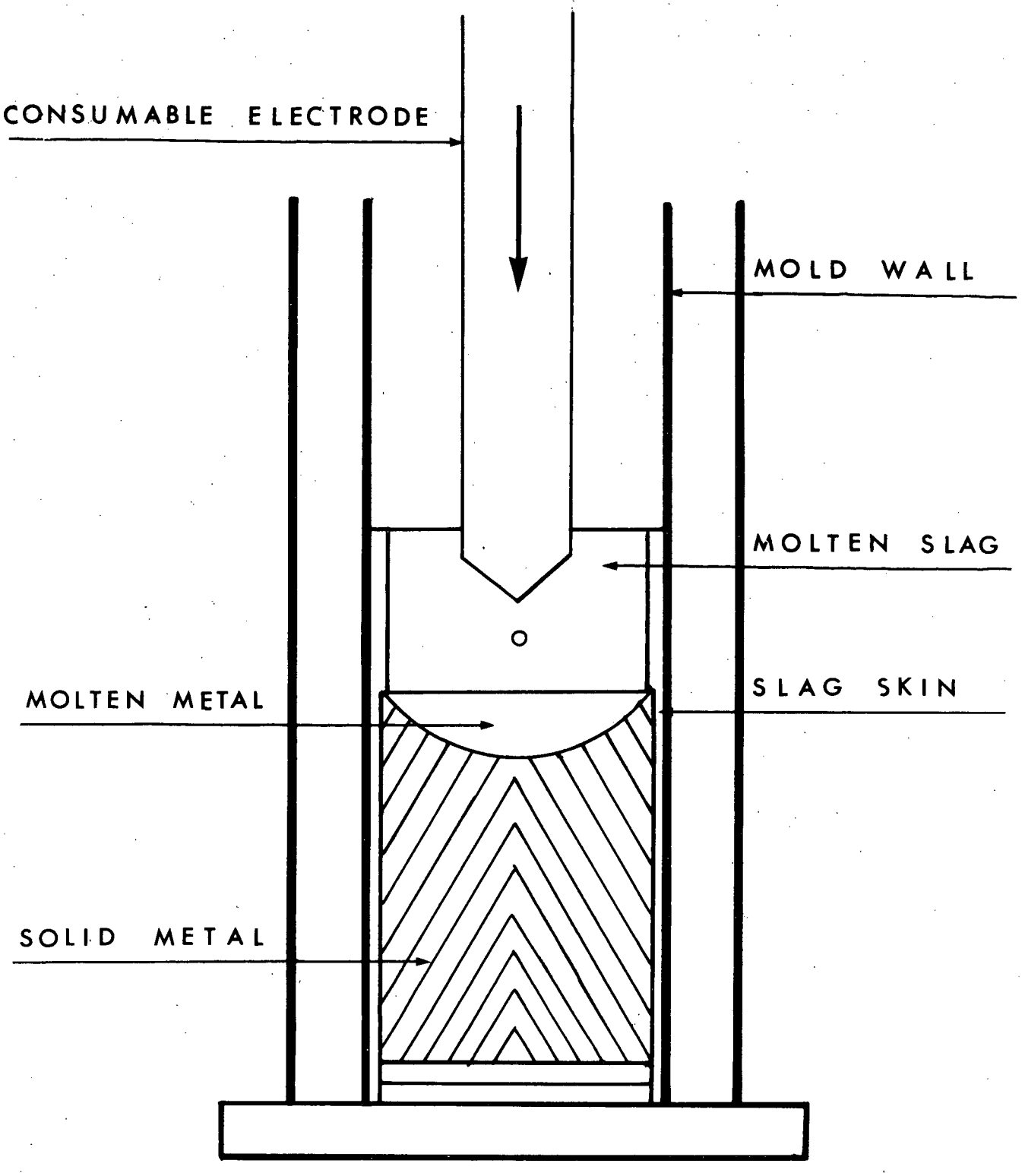

Figure 1 Schematic diagram of electroslag remelting

in intensity and direction of the high density of current in the pool might create electromagnetic fields, capable of stirring the metal pool above the solidifying ingot.

In addition to an eventual electromagnetic stirring, strong convection currents are created by the high temperature gradients existing in the liquid slag. In the central part of the molten flux, the temperature is in the region of 1700°C. At the wall of the watercooled mold, the slag is found to be solid and to form a skin. At the interface liquid slag-solid skin the temperature is the liquidus temperature of the slag (∿1500°C for a 70/30 CaF_2/Al_2O_3 slag). In a mold of 2.5×10^{-2}m radius there is a temperature gradient of the order of 8000°C m^{-1}. Thus, inclusions have many opportunities of being caught in convection currents, to come into contact with the slag and to dissolve or react chemically with it.

It is reported that the removal of inclusions can be accomplished selectively by the use of appropriate fluxes. Thus, the removal of oxide inclusions (excluding silicates) has been observed to be favoured by high process temperatures using slags of high electrical resistance such as 60% CaF_2, 30% CaO, 10% MgO, for instance. The removal of silicates is best achieved by using slags in the system CaF_2-CaO Al_2O_3.[21] On the other hand acidic slags do not favour desulphurization. Holzgruber[22] reports that in lime-alumina-fluorspar-silica slags an increase in the silica content leads to a strong decrease of the alumina contents of the inclusions but on the other hand

to bigger inclusions rich in SiO_2. The alumina content of the inclusions increases with increasing alumina content of the slag.

Some inclusions can dissolve into the slag. Others, before being exposed to the slag, can dissolve in the liquid metal. This last mechanism has been pointed out by Kay[23] and Mitchell.[24] Thus silica or alumina inclusions can dissolve into the metal

$$SiO_2 \rightarrow [Si]_{Fe} + 2[O]_{Fe} \quad (2.1)$$

$$Al_2O_3 \rightarrow 2[Al]_{Fe} + 3[O]_{Fe} \quad (2.2)$$

This behaviour is to be expected from the temperature dependence of the saturation solubility of oxygen, silicon and aluminum according to the equations (as given by Kay[23]

$$\log [\text{wt\% O}]_{Sat} = \frac{6.320}{T} + 2.734 \quad (2.3)$$

$$\log [\text{wt\% Si}][\text{wt\% O}]^2 = \frac{29,150}{T} + 11.01 \quad (2.4)$$

$$\log [\text{wt\% Al}]^2 [\text{wt\% O}]^3 = \frac{64,000}{T} - 20.48 \quad (2.5)$$

From these equations, it can be seen that with increasing temperature more silica and alumina can be taken into solution.

Exchange reactions between the slag and the metal can also take place, such as

$$2(Al_2O_3)_{slag} + 3[Si]_{Fe} = 4[Al]_{Fe} + 3(SiO_2) \tag{2.6}$$

The extent to which such a reaction occurs depends on the composition and the temperature of the slag. Accordingly, an electrode containing alumina or silica inclusions can produce an ingot containing different ratios of these two types of inclusions.

During cooling and solidifying, the metal is supersaturated with the solutes. Accordingly, they precipitate as inclusions.

That solidification occurs mainly axially is an important feature of the electroslag remelting process. Thus inclusions may be pushed ahead of the (solid-liquid) interface and be floated out of the metal. Or they can be entrapped between the dendrites, depending on the interdendritic spacing, controlled by the rate of solidification. The rate of solidification is proportional to the electrode feed rate, as expressed by the relation:

$$V = Ve \frac{d'^2}{D'^2 - d'^2} \tag{2.7}$$

V	rate of solidification of ingot
Ve	electrode feed rate
D'	ingot diameter
d'	electrode diameter

The electrode feed rate, the voltage and the depth of the slag control the depth of the metal pool[16]. Axial dendrites obtained with a shallow bath will reduce the entrapment of inclusions. On the contrary a deep bath, will favour a certain radial crystallisation. Moreover, it will induce convection currents which may help the particles to rise and be absorbed by the slag, but may also reject them towards the solidification front where they can be entrapped.

If the inclusions rise in the metal bath according to Stokes' law, in the absence of convective and electromagnetic stirring their rising speed should be greater than the solidification speed in order for them not to be entrapped by the solidification front. Stokes' law is expressed as follows:

$$v = \frac{2}{9} g r^2 \frac{\rho_m - \rho_{incl.}}{\eta} \qquad (2.8)$$

η	viscosity of the metal
g	gravity constant
r	radius of the particle
ρ_m	density of metal
$\rho_{incl.}$	density of particle

From equations (7) and (8), the size of the inclusions that can be removed may be calculated with respect to the solidification rate, as shown on Figure 2, reproduced from reference 19. From these calculations, it can be seen that convection currents of the order of magnitude of 1 cm/sec are able to move the particles at a higher velocity than that predicted by Stokes' law.

Mitchell and Etienne[20] have also pointed out that during solidification particles of the solid slag skin may sink to the metal surface and give rise to inclusions.

In summary, the removal of inclusions during the electroslag remelting process is held to depend on the composition of the slag and on the solidification rate of the ingot.

Scope of this Work

The object of this work is to derive a model for the behaviour of inclusions during electroslag remelting. As can be expected from the preceding review of the literature, the problem is extensive. Therefore, this study will be limited to the case of Al_2O_3 inclusions.

Two steps are involved:

(1) We must first determine to what extent alumina dissolves in liquid slag. Accordingly, the first step of this work will be to determine the diffusion

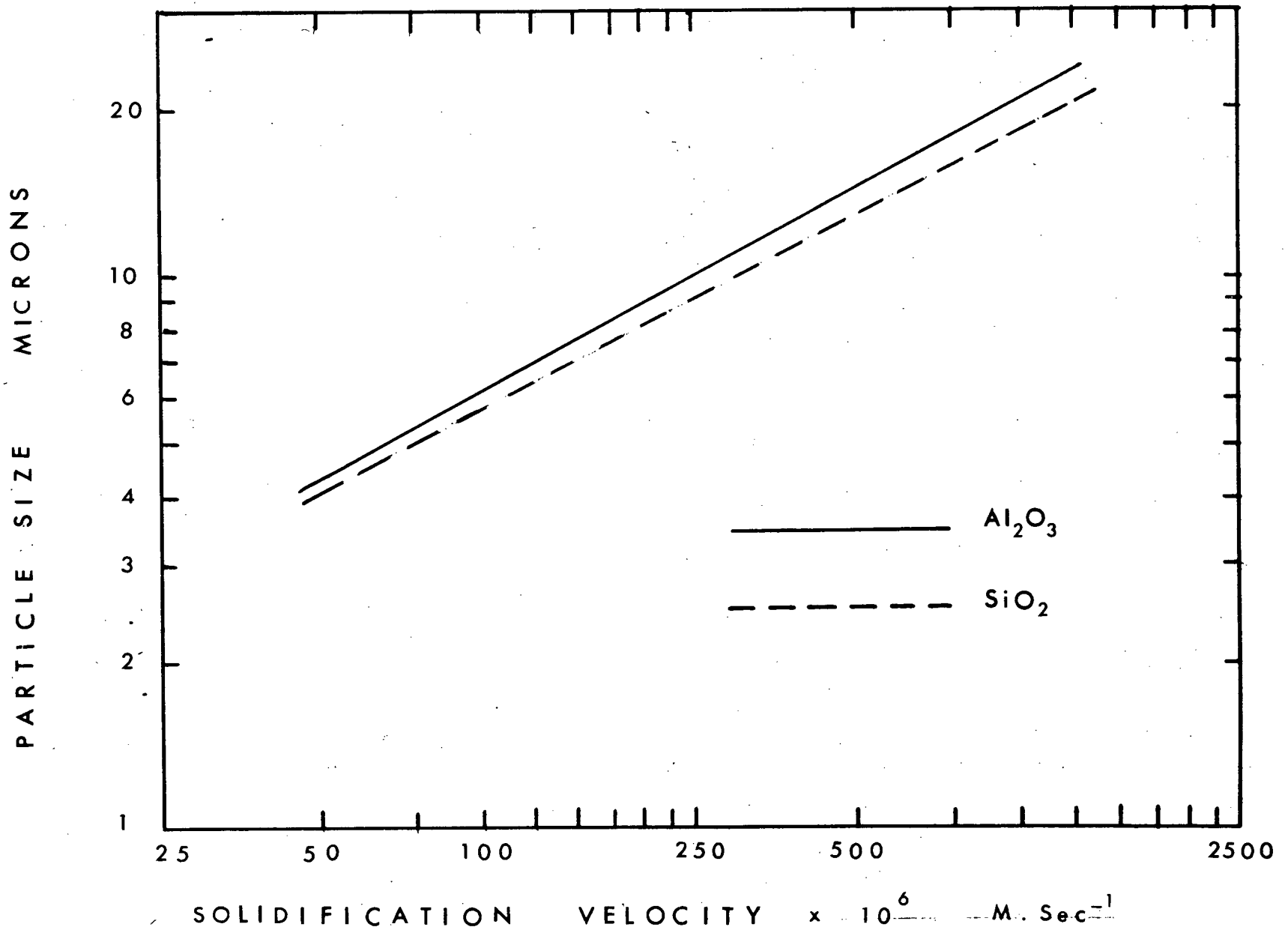

Figure 2 Inclusion removal as a function of the velocity of solidification determined from Stokes' law

coefficient of alumina in CaF_2/Al_2O_3 liquid slags. A numerical value of the diffusion coefficient will enable us to calculate the extent to which Al_2O_3 inclusions dissolve during contact of the liquid metal and the slag with different models assuming different flow conditions.

(2) The second step will be to introduce particles artificially in an electrode and to examine the ingot after electroslag remelting. With the help of the electronmicroprobe, it will be possible to see what kind of inclusions remain or are formed.

III. DETERMINATION OF THE DIFFUSION COEFFICIENT

(1) Mechanism of Diffusion in Molten Salts

The slags used in the electroslag remelting process are mixtures of molten salts, mainly oxides and fluorides. The ionic structure of molten salts suggests some similarities in such properties as conductivity, viscosity and diffusion. Bockris[25] describes liquids not too far above the melting point as having a short range structure similar in many respects to the solid produced on freezing, but lacking the long-range order of the solid. He develops also a "hole" theory of molten salts, also described by Stillinger.[26] Holes would exist to a much greater extent in the liquid than in the solid. Thus, transport processes, such as diffusion or conduction could take place by place exchange of ions or transitions of ions into vacancies appearing next to them.

The Nernst-Einstein equation gives a relation between diffusion and conduction:

$$D_i = \frac{\Lambda_i \, RT}{z_i^2 \, F^2} \tag{3.1}$$

Λ_i	equivalent conductance
z_i	valence of the ion
D_i	self diffusion coefficient
F	Faraday constant
R	thermodynamic constant
T	absolute temperature

Borucka, Bockris and Kitchener[27] have found with molten sodium chloride that this formula is only applicable if diffusion and conduction processes occur by the same mechanism, i.e., migration via single vacancies. He suggested that deviations from this relation could be explained by the fact that diffusion includes displacements of entities which do not contribute to conduction.

The Stokes-Einstein equation relates the coefficient of diffusion to the viscosity of the liquid:

$$D_i = \frac{kT}{6\pi\eta r_i} \tag{3.2}$$

k	Boltzmann's constant
η	viscosity of the liquid
r_i	radius of the ion or molecule that diffuses

Good agreements are found with this formula.[27] For an ionic mechanism, the effective diffusion coefficient is associated with the $D_\pm$ values for individual ions by a relationship of the type:

$$D = \frac{C_+ + C_-}{\frac{C_+}{D_-} + \frac{C_-}{D_+}} \tag{3.3}$$

where $C_\pm$ are the concentrations of the individual ions.

(2) Methods of Determination of Diffusion Coefficients In Slags

Few sources give values of diffusion coefficient of species in molten salts. This is probably due to the fact that no simple method of determining them is known.

Towers and Chipman[28] have measured the coefficient of diffusion of calcium and silicon in a lime-alumina-silica slag, using a radioactive tracer technique. Two slags of same composition are brought into contact, one of them containing the radioactive tracer Ca^{45} or Si^{81}. The experimental values have a large scatter. For instance at 1500°C the scattering spread of points gives for the diffusion coefficient of calcium, values ranging from 1.25 $10^{-10} m^2/sec$ to $4 \times 10^{-10} m^2/sec$.

Russian workers[29,30,31] have been using for many years extensively and with success the rotating disk system to measure the diffusion coefficient of species in liquids. This method has only recently been used by western workers. The technique has also been applied to determine the diffusion coefficient of oxides in molten salts. Table 1 reproduces some of the values found.

The rotating disk has been used in this work to determine the effective diffusion coefficient of Al_2O_3 in binary CaF_2-Al_2O_3 slags. For this reason, it will be discussed in detail in the next section.

TABLE 1

DIFFUSION COEFFICIENTS OF OXIDES IN MOLTEN OXIDE MIXTURES

AT 1600°C (From Reference 28)

slag composition		oxide	diffusion coefficient $Dx10^9$ m^2 sec^{-1}	activation energy $Ex10^{-3}$ Joule $mole^{-1}$
CaO	40 w%	SiO_2	0.72	375
SiO_2	40 w%	MgO	1.10	320
Al_2O_3	20 w%	Al_2O_3	0.17	330
CaO	45 w%	SiO_2	0.87	-
SiO_2	25 w%	MgO	1.20	-
Al_2O_3	30 w%	Al_2O_3	0.24	-
CaO	49 w%	SiO_2	0.76	550
SiO_2	9 w%	MgO	1.80	280
Al_2O_3	42 w%	Al_2O_3	0.30	-
CaO	48 w%	SiO_2	2.30	-
SiO_2	0 w%	MgO	3.50	-
Al_2O_3	52 w%	Al_2O_3	1.10	-

(3) <u>The Rotating Disk System</u>

Levich[32] has solved the convective diffusion equation under the following assumptions:

a) the solute concentration of the liquid is independent of radial and angular position, but is solely dependent on the axial distance from the disk surface.

b) also the steady state transport across the diffusion layer is assumed to be established rapidly.

The equation can then be written in cylindrical coordinates:

$$V_z\ (z)\ \frac{dC}{dz} = D\ \frac{d^2C}{dz^2} \qquad (3.4)$$

where $V_z(2)$ is the axial component of the velocity of the liquid, D the solute diffusion and C the solute concentration. For high Schmidt numbers ($D << \nu$) the solution of the equation has been found to be:

$$J = 6.2\ D^{2/3}\ \nu^{-1/6}\ \omega^{1/2}\ (C_{Sat} - Co) \qquad (3.5)$$

J	maximum (initial) mass flux of solute in kg $m^{-2}sec^{-1}$
ν	kinematic viscosity of the liquid in $m^2\ sec^{-1}$
ω	angular velocity of the disk in radians/sec
C_{Sat}	solubility of the solute in the liquid in kg m^{-3}
Co	initial solute concentration in the liquid in kg m^{-3}

The thickness of the diffusion boundary layer is given by:

$$\delta = \frac{D(C_{Sat} - C_o)}{J} \tag{3.6}$$

or substituting (3.5) into (3.6)

$$\delta = .161 \left(\frac{D}{\nu}\right)^{1/3} \left(\frac{\nu}{\omega}\right)^{1/2} \tag{3.7}$$

(4) Practical Applications of the Rotating Disk System for the Determination of Diffusion Coefficients

Besides the determination of diffusion coefficients in molten salts previously mentioned[29,30,31], the rotating disk technique has been applied to many systems. Thus, Kassner[33] has measured the coefficient of diffusion of tantalum in tin. Olsson, Perzak and Koump[34] have determined the diffusion coefficient of alumina in pure molten iron oxide. In both cases good agreement was found with the prediction of a rate of dissolution proportional to $\omega^{1/2}$ (square root of the angular velocity).

Riddiford[35] makes comments on the practical rotating disk system and gives a review of the literature on its applications. The theory assumes that the disk is of infinite radius and zero thickness. In practice, in order to get accurate results, the experimenter must try to get as close as possible to these ideal conditions. The disk must not be stirred too close to the container, to insure flow conditions close to the ideal case. The edge effect must be reduced as much as possible by using disks which are thin with respect to their radius. A ratio of 30 between the radius of the disk and its thickness is

quoted as eliminating the edge effect. In addition, the diameter of the stirring shaft should be as small as possible. A ratio of 3.5 of the diameter of the disk to that of the shaft is a minimum to get suitable results. Other design factors are the smoothness of the disk and the eccentricity of the rotating system. There is also probably interaction between the fluid flow in the upper and lower halves of the system. All these factors have an influence on the accuracy of the results. The system must be designed carefully in order to minimize all these effects.

IV. THERMODYNAMICS OF THE SYSTEM CaF_2 - Al_2O_3

The experimental determination of the diffusion coefficient of alumina in CaF_2 - Al_2O_3 mixtures, using the rotating disk system, was conducted with 70/30 and 80/20 CaF_2/Al_2O_3 slags contained in graphite cruicibles under an atmosphere of argon. Two points must be studied closely:

a) the stability of the slag with respect to the formation of volatile compounds between CaF_2 and Al_2O_3 and of carbides with the graphite of the cru cible

b) the liquidus line of the binary CaF_2 - Al_2O_3 diagram.

(1) Stability of the CaF_2 - Al_2O_3 Mixture

Mitchell[24] has studied the problem of the stability of the CaF_2 - Al_2O_3 system. The following reactions must be examined for our practical case:

$$3\ CaF_2 + Al_2O_3 = 2\ AlF_3\ (g) + 3\ CaO \quad (4.1)$$

$$CaF_2 + Al_2O_3 + 2\ C(gr) = 2\ AlF_{(g)} + CaO + 2\ CO \quad (4.2)$$

$$(CaO)_{CaF_2} + 3\ C(gr) = (CaC_2)_{CaF_2} + CO \quad (4.3)$$

$$2\ (Al_2O_3)_{CaF_2} + 9\ C\ (gr) = (Al_4C_3)_{CaF_2} + 6\ CO \quad (4.4)$$

The free energies of reaction can be calculated from the data of free energy of formation of oxides[36], carbides[37], and

fluorides[38]. They have been calculated at 1500°C and 1600°C, which is the range of temperature of the experiments.

For the formation of AlF_3 (g) with the stochiometry of reaction (4.1), the free energies are:

at 1500°C $\Delta F^1_{1500} = + 575 \times 10^3$ Joules (138 Kcal)

at 1600°C $\Delta F^1_{1600} = + 510 \times 10^3$ Joules (122 Kcal)

The CaF_2 - Al_2O_3 binary system forms a eutectic. So the values of the activities should be slightly higher than the ideal values. We can take $a_{Al_2O_3} \simeq a_{CaF_2} \simeq 1$. Furthermore, the industrial CaF_2 used is found to contain about 1% CaO. So the activity of CaO can be assumed to be $a_{CaO} \simeq 10^{-2}$. This gives an estimation of the partial pressure of AlF_3

at 1500°C $P_{AlF_3} = 0.3 Nm^{-2}$ (3×10^{-6}atm)

at 1600°C $P_{AlF_3} = 7 Nm^{-2}$ (7×10^{-5}atm)

The formation of AlF_3 can therefore be neglected. For the formation of AlF with the stochiometry of reaction (4.2), the free energies are:

at 1500°C $\Delta F^2_{1500°C} = + 368 \times 10^3$ Joules (88 Kcal)

at 1600°C $\Delta F^2_{1600°C} = + 300 \times 10^3$ Joules (72 Kcal)

Assuming that in the graphite crucible, under an argon atmosphere, P_{CO} is approximatively $10^4 Nm^{-2}$ (10^{-1}atm) and taking

for the same reasons as previously $a_{CaO} \simeq a_{Al_2O_3}$, an estimation of P_{AlF} can be obtained

at 1500°C $P_{AlF} = 100\ Nm^{-2}\ (10^{-3} atm)$

at 1600°C $P_{AlF} = 500\ Nm^{-2}\ (5x10^{-3} atm)$

The formation of AlF(g) can also be neglected. By comparison, the vapor pressure of CaF_2 at these temperatures has been calculated, taking the results of Shulz and Searcy[39].

at 1500°C $P_{CaF_2} = 30\ Nm^{-2}\ (3x10^{-4} atm)$

at 1600°C $P_{CaF_2} = 150\ Nm^{-2}\ (1.5x10^{-3} atm)$

The vaporization of CaF_2 is also negligible. The free energy of reaction for the formation of CaC_2 with the stochiometry of the reaction (4.3) has been calculated:

at 1500°C $\Delta F^3_{1500°C} = +\ 142x10^3$ Joules (34 Kcal)

at 1600°C $\Delta F^3_{1600°C} = +\ 109x10^3$ Joules (26 Kcal)

Taking also $P_{CO} \simeq 10^4\ Nm^{-2}\ (10^{-1}$ atm) and assuming that a_{CaO} is not greater than 10^{-1}, the activity of CaC_2 can be estimated:

at 1500°C $a_{CaC_2} = 8x10^{-3}$

at 1600°C $a_{CaC_2} = 3x10^{-2}$

The formation of CaC_2, therefore, is not very significant.

The free energy of reaction for the formation of Al_4C_3 with the stochiometry of reaction (4.4) has been calculated:

at 1500°C $\Delta F^4_{1500°C} = 492 \times 10^3$ Joules (114 Kcal)

at 1600°C $\Delta F^4_{1600°C} = 310 \times 10^3$ Joules (74 Kcal)

Taking also $P_{CO} \simeq 10^4\ Nm^{-2}$ (10^{-1}atm) and $a_{Al_2O_3} \simeq 1$, this gives for $a_{Al_4C_3}$

at 1500°C $a_{Al_4C_3} = 10^{-8}$

at 1600°C $a_{Al_4C_3} = 2.5 \times 10^{-3}$

No significant quantity of Al_4C_3 can be formed.

(2) Equilibrium Diagram For the System CaF_2 - Al_2O_3

In the CaF_2 - Al_2O_3 system, the presence of compounds between CaO and Al_2O_3 such as CaO - Al_2O_3, CaO - 2 Al_2O_3, 3 CaO - 5 Al_2O_3 and CaO - 6 Al_2O_3 can be explained by the formation of CaO by reactions (4.1) and (4.2) and also the following reaction:

$$CaF_2 + H_2O = (CaO)_{CaF_2} + 2\ HF\ (g) \qquad (4.5)$$

It is therefore difficult to get a binary diagram for the system CaF_2 - Al_2O_3 because of the formation of different amounts of CaO and, thereby, of calcium aluminates. In the literature different phase diagrams have been proposed and different phases identified.

Kuo Chu-Kun and Yen Tung-Sheng[40] have studied the phase equilibrium relationships in the system CaF_2 - Al_2O_3 by the quenching method, and they have identified the phase CaO - 2 Al_2O_3. They cite other workers as finding solid solutions of CaF_2 and Al_2O_3 (Pascal) or compounds $CaAl_2O_3F_2$ and CaF_3 - 5 Al_2O_3.

For the present study, the knowledge of an accurate binary diagram is very important in order to calculate the diffusion coefficient. A binary diagram has been determined from the cooling curves of different compositions of the binary CaF_2 - Al_2O_3. Such a determination is difficult, mainly because, as the concentration of Al_2O_3 increases, the break on the cooling curve for starting solidification becomes less noticeable. Also there may be a substantial amount of supercooling. The diagram obtained is shown on Figure 3. Figure 4 gives a comparison of this diagram with those obtained by Kuo Chu-Kun and Yen Tung-Sheng and Pascal.[40] Extrapolation to 100% Al_2O_3 of the liquidus line obtained in this work would give a temperature around 1870°C which does not correspond to the melting point of Al_2O_3 (m.p. 2040°C), but might correspond to the incongruent melting point of calcium hexaluminate. This compound has been studied by Buist[41]. Calcium hexalumimate forms in the binary system CaO - Al_2O_3 with 9.3% of CaO, so that in the mixture CaF_2 - Al_2O_3 for compositions 80/20 and 70/30 of these two components, a relatively small amount of CaO (2 to 3%) could lead to the formation of calcium hexaluminate. Therefore, theoretically the diagram could be in fact a CaF_2 -

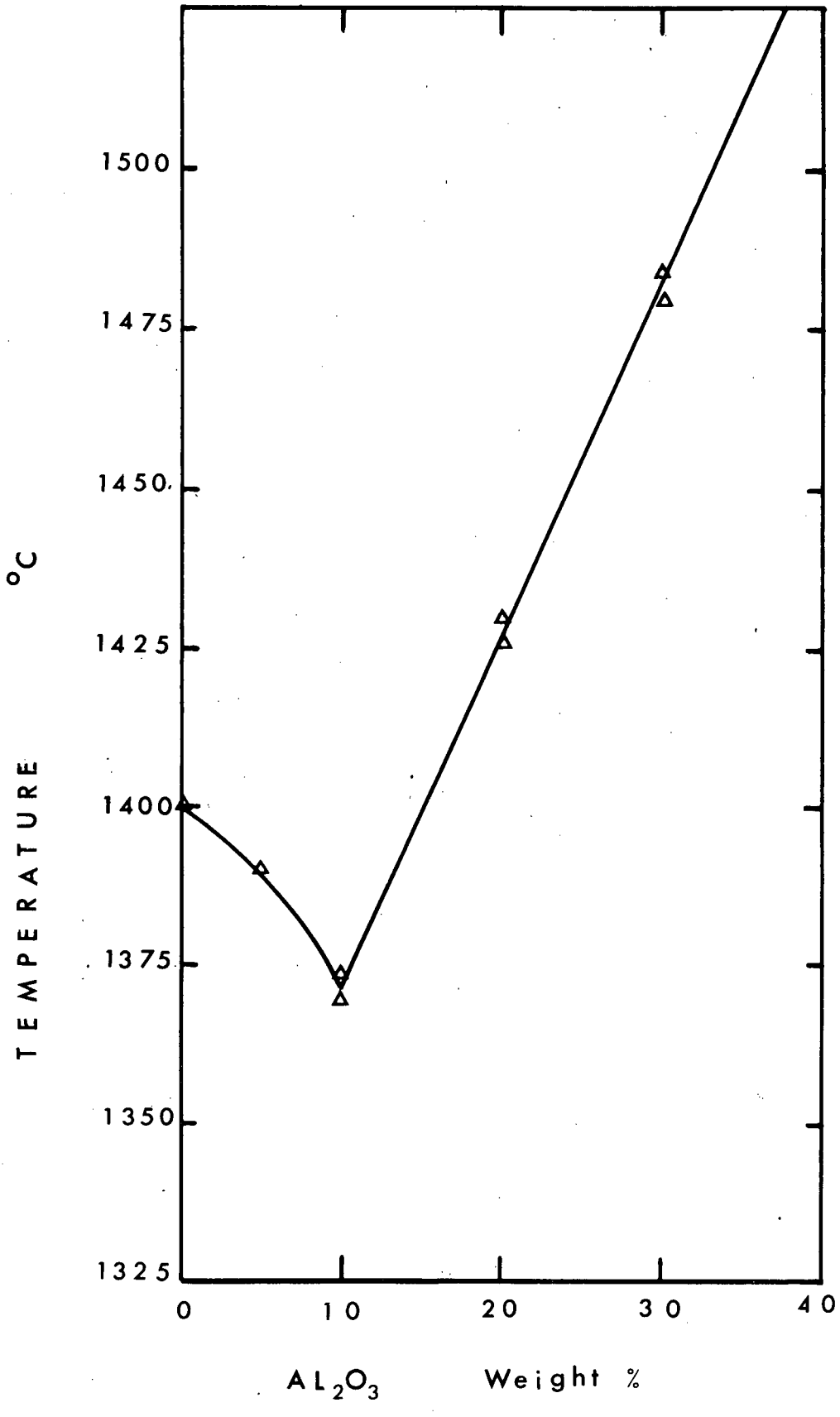

Figure 3 CaF_2 - Al_2O_3 binary diagram determined in this work

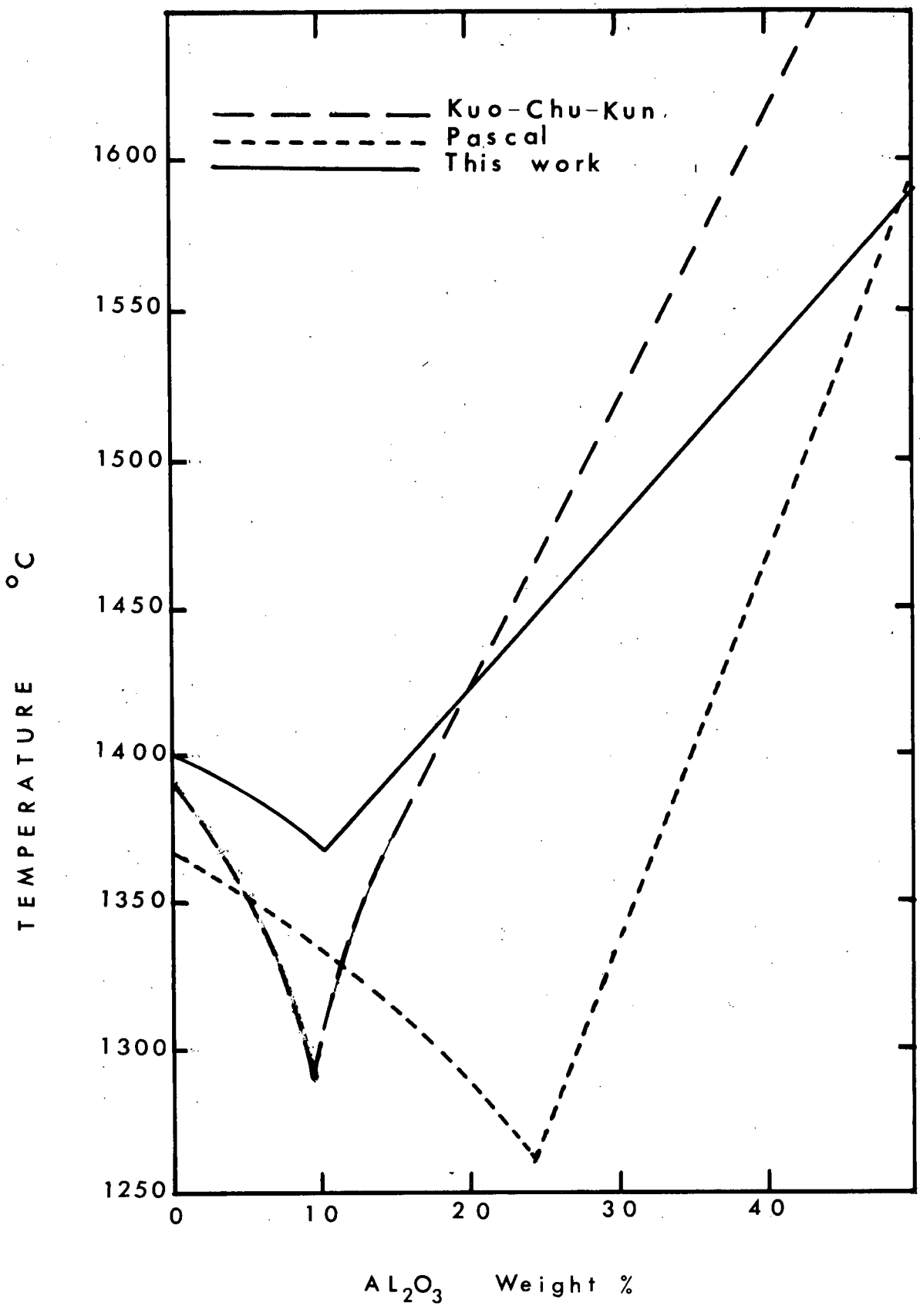

Figure 4 Comparison of the CaF_2 - Al_2O_3 binary diagram determined in this work with other determinations

$CaO - 6\ Al_2O_3$ pseudo-binary diagram.

The solid mixture of a 60/40 CaF_2/Al_2O_3 slag has been examined by X-Ray powder diffraction. The results are reported in Appendix I. The lines of CaF_2 appear very clearly. Those of Al_2O_3 are weak and diffuse. Some lines could not be identified. They do not correspond to any reported set of lines for calcium aluminates. It should be also pointed out that the X-Ray powder data for calcium hexaluminate given in the literature are often contradictory. In addition they are very close to the Al_2O_3 data. There is a substantial solubility between calcium hexaluminate and alumina and,as they are of similar structure, the powder diffraction lines would move slightly but not be of markedly different spacings going from alumina to calcium hexaluminate.

V. EXPERIMENTAL DETERMINATION OF THE DIFFUSION COEFFICIENT

(1) Description of the Apparatus

The apparatus is shown schematically on Figure 5. A graphite crucible (3.5 10^{-2}m in diameter, 5 10^{-2}m high) containing the slag is heated by an induction coil outside a silica tube. An alumina sheath protecting a thermocouple (platinum, platinum 10% rhodium) holds the crucible in the middle region of the coil. The crucible is surrounded on its sides, above and underneath by two layers of graphite felt. The silica tube rests on a water-cooled brass plate. The alumina thermocouple sheath is held in a pyrex tube; it passes through a copper tube brazed in the middle of the brass plate and is held by a sliding 0-ring seal. Thus, the crucible which rests on the alumina thermocouple sheath may be positioned in the apparatus along a vertical axis. The pyrex tube is provided with an inlet for the argon. Another water-cooled brass plate closes the silica tube at the top. It is provided with an outlet for the argon and it holds the rotating shaft. This is composed of two parts. The molybdenum shaft (2.4 10^{-3}m in diameter) holds the alumina disk on a plate (6.4 10^{03}m in diameter) fixed at its tip. A square shaped tip ensures that the disk spins at the same speed as the shaft. A pin which can be removed after each run holds this molybdenum shaft to a steel shaft. A pulley fixed at the top of the shaft holds it on brass top plate. A rubber belt connects this pulley to the motor. The motor is a "Motomatic" E-550 MGHP equipped with a tachogenerator feed-back speed control system. Its speed ranges between 0 to 500 r.p.m.

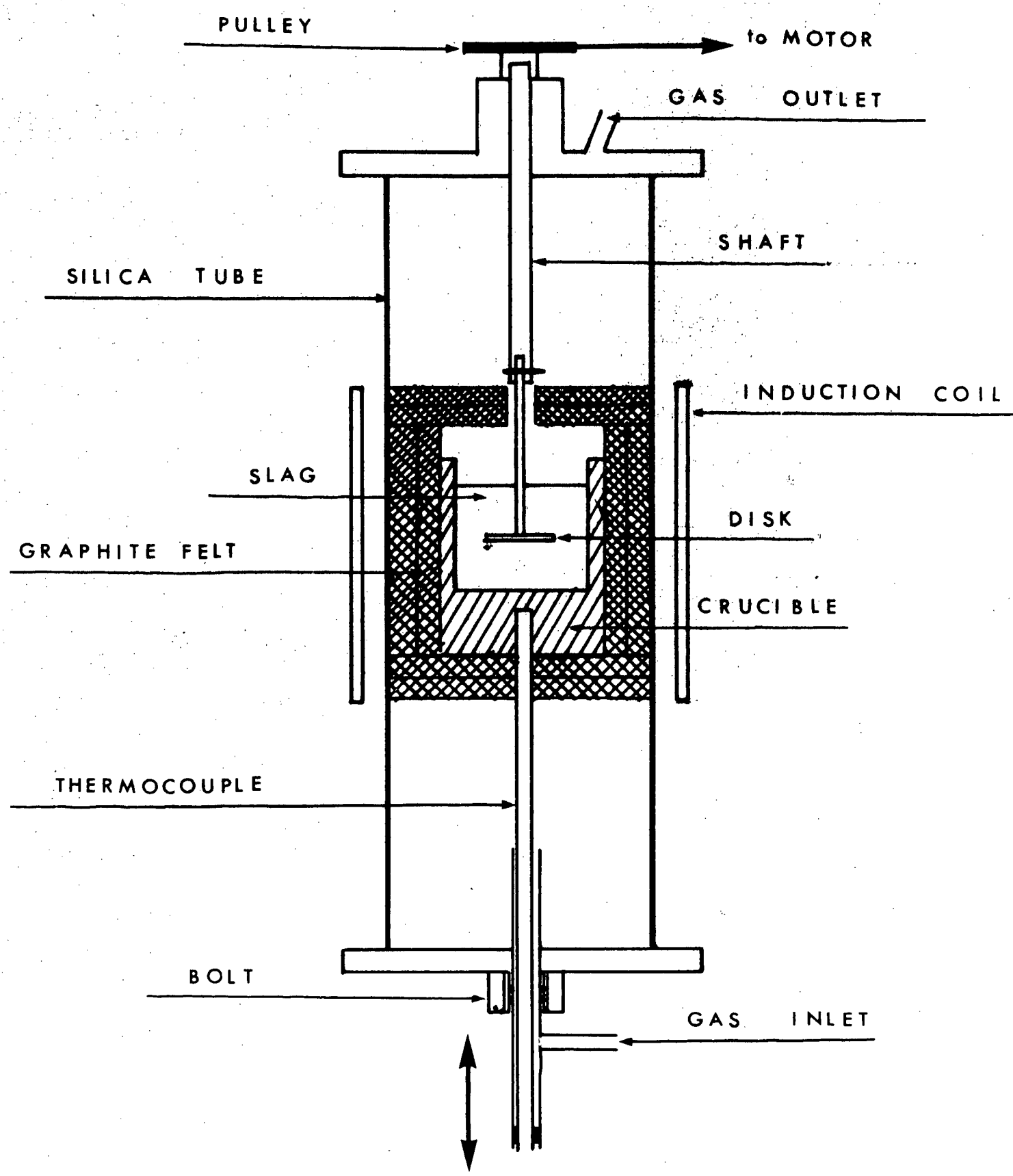

Figure 5 Schematic diagram of the rotating disk apparatus

(2) Preparation of the Disks

The disks were cut from sintered alumina plates with the ultrasonic drill. Their diameter was 2.05 10^{-2}m and their thickness 5 10^{-4}m and they had a square hole in their center (.39 10^{-4}m x .39 10^{-4}m) to fit the square shaped tip of the molydenum shaft. A special tool was made for the ultrasonic drill in order to cut at the same time the disk and the square hole out of the alumina plates. This ensures that rotational eccentricity is minimized.

(3) Experimental Procedure

The components of the CaF_2 - Al_2O_3 slag were placed in the graphite crucible, CaF_2 in prefused lumps and Al_2O_3 in powder. The disk was set on the shaft and several rings of molybdenum wire rested on its upper surface in order to ensure that the disk did not float on the surface of the slag by surface tension, when introduced into the slag. The crucible was set in the furnace just under the disk. The temperature in the furnace was controlled by the platinum - platinum 10% rhodium thermocouple. The temperature of the slag was determined with a tungsten 3% rhenium - tungsten 25% rhenium thermocouple protected by a boron nitride sheath. Once the slag was brought to the chosen temperature and maintained at this temperature, the alumina tube was lifted in order to immerse the rotating disk into the slag. At the same time a timer was started. At the end of the run, as the alumina tube holding the crucible was lowered, the timer was stopped.

The disks were spun for times ranging between 24 and 65 seconds and rotating speeds between 50 r.p.m. and 400 r.p.m. Because of the electromagnetic forces on the shaft created by the induction field in the coil, it was sometimes difficult to stabilize the rotating speed at its set value. After cooling down the furnace, the disk was found covered with some slag which had frozen on its upper and lower surfaces. This frozen slag was dissolved in a mixture of molten Na_2CO_3 and K_2CO_3 (anhydrous) contained in a platinum crucible with about the eutectic composition of these two salts (eutectic composition 44 mol% of K_2CO_3, eutectic temperature 710°C).[42] The mixture Na_2CO_3 - K_2CO_3 dissolves CaF_2 but not Al_2O_3. It took 15 to 30 minutes to dissolve the slag, then the disk was washed in a solution of hydrochloric acid which dissolves Na_2CO_3 and K_2CO_3. A preliminary test had been done with a piece of alumina plate which had not been dissolved in the CaF_2 - Al_2O_3 slag in order to ensure that it did not dissolve during cleaning in the Na_2CO_3 - K_2CO_3 mixture and in the acid solution. The disks could then be weighed and their weight loss calculated.

(4) Results

The experiments were conducted in a 70/30 CaF_2/Al_2O_3 slag at temperatures measured at 1518°C and 1509°C and in a 80/20 CaF_2/Al_2O_3 slag at 1500°C. The experimental data are given in Appendix II, III and IV. The mass flux per second in the three different cases has been plotted versus the square

root of the rotating speed of the disk on Figures 6, 7 and 8.

The diffusion coefficient can be calculated knowing the slope of the least square line passing through the origin and using Levich's equation (3.5).

$$J = 6.2\ D^{2/3}\ \nu^{-1/6}\ \omega^{1/2}\ (C_{Sat} - C_o) \qquad (3.5)$$

First the least square line passing through the experimental points was calculated but in order to fit equation (3.5), the least square line passing through the origin of the coordinates was also determined by adding several times the origin in the statistics of the experimental points. The working surface of the disk was calculated from the characteristics of the disk since in equation (3.5) J is the mass flux per unit time and per unit area.

The values of the viscosity were taken from Joshi's and Mitchell's results[43] as known at this date. As the temperature variation of the viscosity was not known the value for 1580°C was taken. In order to calculate the kinematic viscosity $\nu = \frac{\eta}{d}$, the density of the slag was calculated using the density of calcium fluoride measured by Kirshenbaum, Cahill and Stokes[44] and the density of alumina. Since the partial volume of solution of alumina in CaF_2 is not known, it was supposed that alumina dissolved in CaF_2 occupies the same volume as pure solid alumina. The values of the density are therefore an approximation. ω (rotating speed in radians per sec) is related to

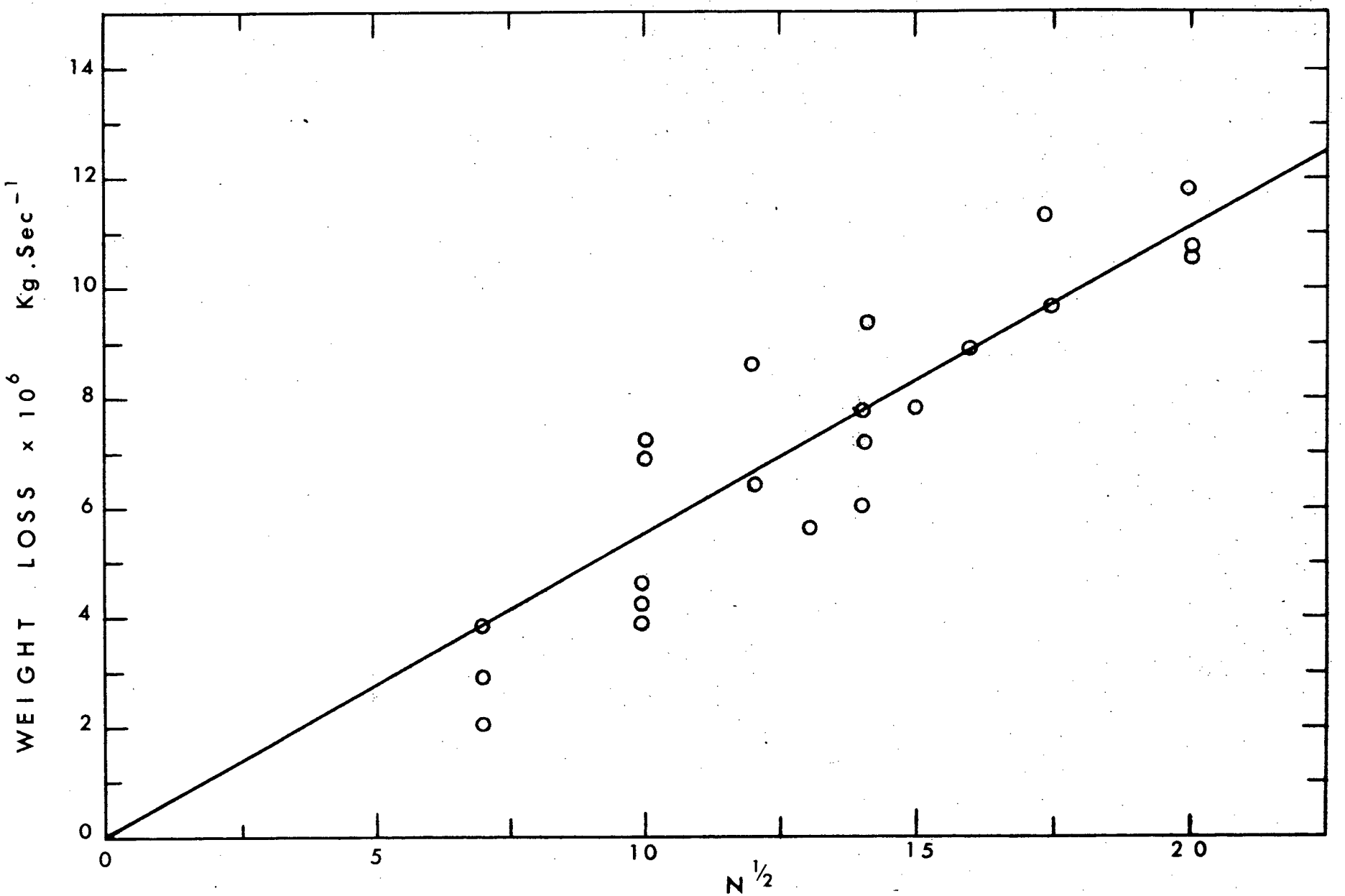

Figure 6 Weight loss of the alumina disks versus the square root of the rotating speed in 70/30 CaF_2/Al_2O_3 slag at 1518°C

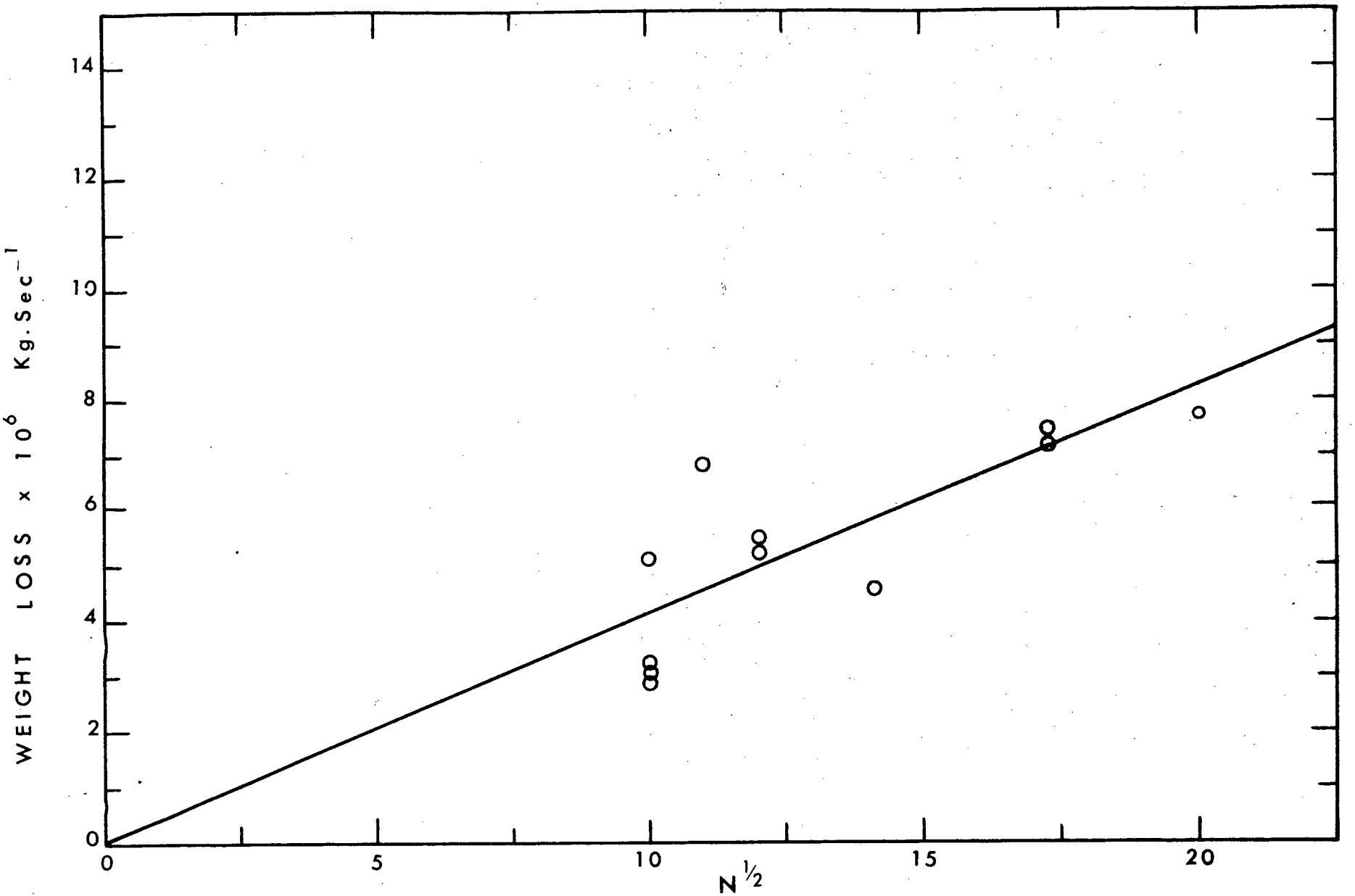

Figure 7 Weight loss of the alumina disks versus the square root of the rotating speed in 70/30 CaF_2/Al_2O_3 slag at 1509°C

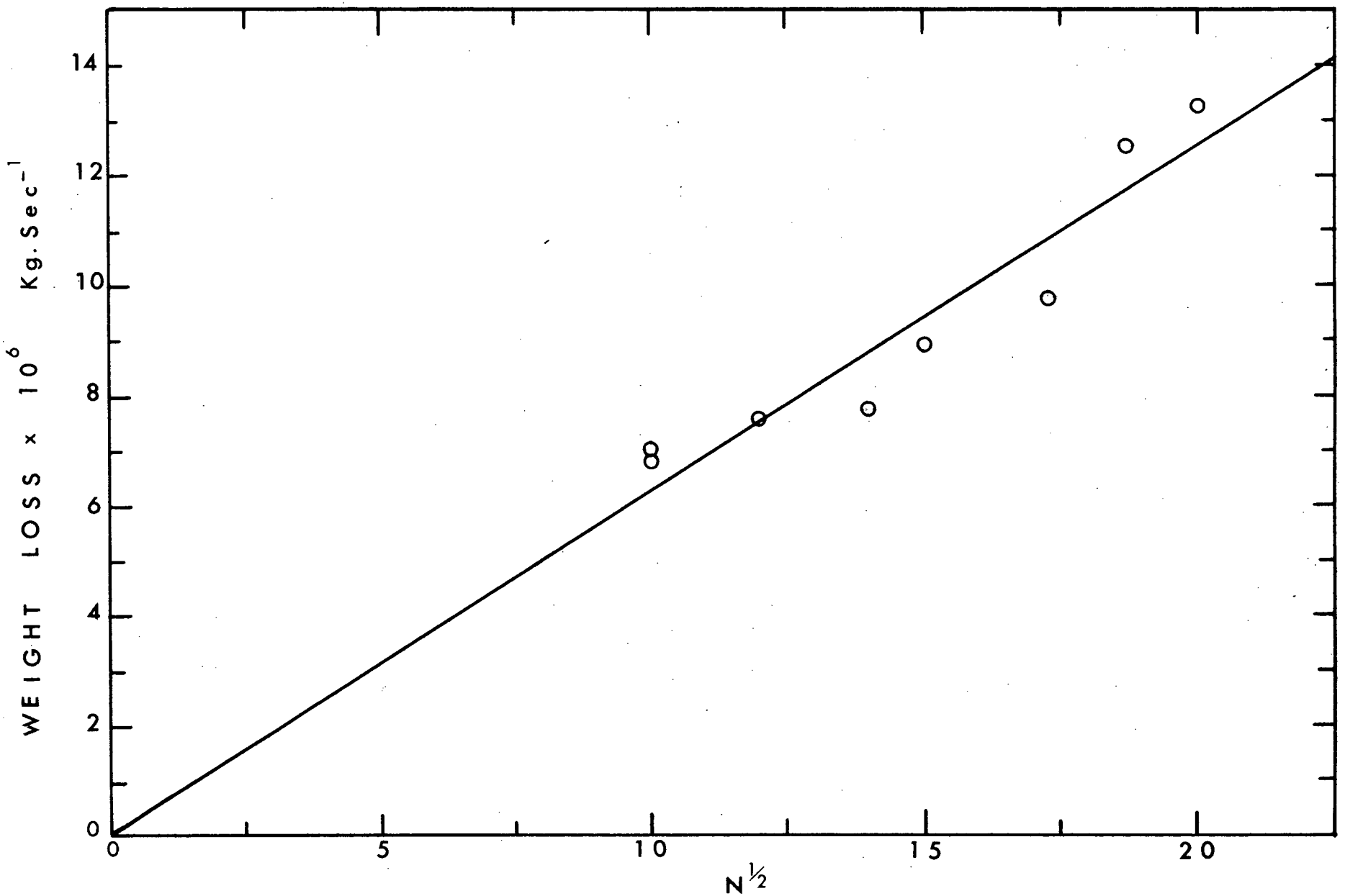

Figure 8 Weight loss of the alumina disks versus the square root of the rotating speed in 80/20 CaF_2/Al_2O_3 slag at 1500°C

the rotating speed N in revolutions per minute by the relation

$$\omega = \frac{2\pi N}{60}$$

C saturation was taken from the binary diagram at the temperature of the experiment and was multiplied by the density of the slag in order to have it in weight per unit volume of solution.

C_o is the concentration of the slag in Al_2O_3 in weight per unit volume. Table 2 gives a summary of the results.

(5) Discussion of the Results

The results are discussed from three points of view, from the point of view of the accuracy of the measurements, from the point of the accuracy of the calculations of the diffusion coefficient and from the point of view of the mechanisms involved in the diffusion process.

a) Accuracy of the measurements

The points are scattered around the least square lines on Figures 6, 7 and 8. This can be explained by the difficulty in maintaining the crucible and its content at a stable temperature. When the crucible was raised to immerse the rotating disks, slight temperature changes ± 10°C could be recorded due to the fact that the crucible entered a region of the induction coil of greater flux density, that the disk and the shaft holding it were not at the same temperature as the liquid slag and

TABLE 2

DETERMINATION OF THE DIFFUSION COEFFICIENT OF ALUMINA IN CaF_2 - Al_2O_3 SLAGS

Slag	least square fit $Jx10^6$ kg sec^{-1}	correlation coefficient	least square line passing through the origin $Jx10^6$ kg sec^{-1}	standard error for the slope 95% confidence	working surface of the disk m^3	η kg m^{-1} sec^{-1}	$dx10^{-3}$ kg m^{-2}	$Dx10^9$ m^2 sec^{-1}
70/30 CaF_2/Al_2O_3 1518°C	$0.63\sqrt{N}-1.18$	0.90	$0.55\sqrt{N}$	± 0.14	$6.3x10^{-6}$	0.06	2.69	8.5
70/30 CaF_2/Al_2O_3 1509°C	$0.39\sqrt{N}+0.29$	0.79	$0.41\sqrt{N}$	± 0.18	$6.3x10^{-6}$	0.06	2.69	8.1
80/20 CaF_2/Al_2O_3 1500°C	$0.61\sqrt{N}+0.24$	0.94	$0.63\sqrt{N}$	± 0.06	$6.3x10^{-6}$	0.07	2.62	4.0

that the inertia of the control system of the furnace made it unable to stabilize the temperature quickly to its set value. Furthermore, the mass flux of material is related to the concentration gradient by a relation of the form

$$J = \frac{D}{\delta} \Delta C$$

where D is the diffusion coefficient and δ the diffusion boundary layer. These two quantities are not significantly affected by a change of temperature of ± 10°C. But the concentration gradient (in weight of material per unit volume of slag) is proportional to the concentration gradient in weight per cent of mixture as determined on the binary diagram on Figure 3. For instance, for the experiment at 1518°C in a 70/30 CaF_2/Al_2O_3 slag:

$$\Delta C \propto 6.5 \times 10^{-2} \text{ w \%}$$

An error of ±10°C makes the value vary between 4.5 w% and 8.5 w%. This corresponds to an error of ±20% on the mass flux of material that dissolves At 1509°C this uncertainty is still larger,as the concentration gradient is smaller The correlation coefficient is 0.79 instead of 0.90 at 1518°C. For the experiment in a 80/20 CaF_2/Al_2O_3 slag the concentration gradient is larger (proportional to 14 weight%) and an uncertainty of ±10°C on the temperature has a much less detrimental effect on the accuracy of the determination of J(±10%). The

points are much less scattered and the correlation coefficient better (0.94).

The least square line passing through the experimental points has been first calculated as: $y = ax + b$. The b value is found to be statistically significant only for the experiment in a 70/30 CaF_2/Al_2O_3 slag.

b) Error of calculation of the diffusion coefficient

The diffusion coefficient has been calculated using Levich's equation (3.5)

$$J = 6.2 \quad D^{2/3} \; \nu^{-1/6} \; \omega^{1/2} \quad (C_{Sat} - C_o) \tag{3.5}$$

By logarithmic derivation of this equation, the error on the diffusion coefficient has been calculated:

$$\frac{\Delta D}{D} = \frac{3}{2} \; \frac{\Delta (J/\omega^{1/2})}{(J/\omega^{1/2})} + \frac{1}{4} \; \frac{\Delta \nu}{\nu} + \frac{3}{2} \; \frac{\Delta (C_{Sat} - C_o)}{(C_{Sat} - C_o)}$$

In this relation:

$-\dfrac{\Delta \; (J/\omega^{1/2})}{(J/\omega^{1/2}}$ is the relative error on the determination of the slope of the least square line. This error has been estimated statistically for 95% confidence. The standard error for 90% confidence is about 2/3 of the error for 95% confidence.

– $\frac{\Delta\nu}{\nu}$ is the error on the kinematic viscosity.

$$\nu = \frac{\eta}{d}$$

where η is the dynamic viscosity measured by Joshi and Mitchell[43] and d the density of the slag

$$\text{So} \quad \frac{\Delta\nu}{\nu} = \frac{\Delta\eta}{\eta} + \frac{\Delta d}{d}$$

The error on the dynamic viscosity is composed of the experimental error (not yet determined) and of the error coming from the fact that no dependence of the temperature could be taken into account.

$\frac{\Delta d}{d}$ is the error on the determination of the density of the slag. As discussed previously, only an estimation of this quantity could be made. Yet in equation (4.1), $\frac{\Delta\nu}{\nu}$ is affected by a coefficient $\frac{1}{4}$. So, it does not seem that the contribution of the term $\frac{1}{4}\ \frac{\Delta\nu}{\nu}$ on the total error is very large.

– $\frac{\Delta(C_{Sat}-C_o)}{C_{Sat}-C_o}$ is the relative error of determination of the diffusion concentration gradient expressed in weight of solute per unit volume of slag.

$C_{Sat}-C_o$ is the gradient read on the binary diagram (Figure 3) multiplied by the density of the slag. Therefore it

is directly related to the accuracy of the determination of the binary diagram and, as discussed previously, it can be important since an error of ± 10°C in the determination of the equilibrium diagram can give a relative error on the concentration gradient of ± 20%. From our determination of the binary diagram the error of measurement can be estimated at ± 3°C for w% of Al_2O_3 less than 30%. This would give an error of 7% on the calculation of the diffusion coefficient.

In conclusion the theoretical error on the determination of the diffusion coefficient could be of the order of 40 to 50% for the diffusion coefficient of Al_2O_3 in a 70/30 CaF_2/Al_2O_3 slag at 1518°C.

c) Discussion of the mechanism of diffusion

The measured values of the diffusion coefficient have been compared to the values calculated from the Stokes-Einstein and Nernst-Enstein equations. Using the Stokes-Einstein equation and taking into consideration the different ions (Al^{3+} and O^{2-}), the closest value to the measured value of the diffusion coefficient at 1518°C in a 70/30 CaF_2/Al_2O_3 slag is that for the ion Al^{3+} ($1.2\ 10^{-9}\ m^2sec^{-1}$ compared to the measured value $8.5x10^{-9}\ m^2sec^{-1}$). The validity of the application of the Stokes-Einstein equation can be questioned because it assumes a dilute solution, which is not the case in a 70/30 CaF_2/Al_2O_3 slag. In addition aluminum is likely to

be found in solution tied up with oxygen, forming AlO_2^- more numerous and bigger than the Al^{3+} ions.

The Nernst Einstein equation gives a better approximation of the diffusion coefficient. The conductivity of a 70/30 CaF_2/Al_2O_3 slag can be estimated as 150 mho m^{-1} according to Evseev's[45] and Kammel's and Winterharger's[46] results. The O^{2-} ions, the transport number of which can be estimated as about 0.6, can be assumed to be responsible for the ionic diffusion since the AlO_2^- ions are much bigger (transport number $\simeq$ 0). This would give a diffusion coefficient $D_{O^{2-}}$ of $4 \times 10^{-9} m^2$ sec^{-1}, which is less than half the value measured for the diffusion of Al_2O_3 in the slag (8.5×10^{-9} m^2 sec^{-1}). Still it is a better approximation than that given by the Stokes-Einstein equation. The models of rigid spheres moving in a viscous flow do not apply very well to molten salts.

VI. DISSOLUTION OF INCLUSIONS DURING ELECTROSLAG REMELTING

The purpose of the determination of the diffusion coefficient of alumina in CaF_2 - Al_2O_3 slags was to enable us to predict the extent to which alumina inclusions in steels would dissolve in the slag during electroslag remelting. First calculations have been made on different models approaching the conditions of electroslag remelting. Then experiments have been done using the University of British Columbia's electroslag unit with particles of alumina artificially introduced in the electrode.

(1) Dissolution of a Sphere

Readey and Cooper[47] have derived the differential equations governing the dissolution of a sphere of finite radius controlled by molecular diffusion, taking into consideration the effects of the moving boundary and the resulting radial convective transport.

These equations have been solved numerically with the computer. Using the curves that they have drawn, it is possible to assess the order of magnitude of the time necessary for the complete dissolution of a sphere. The temperature chosen for this assessment is 1515°C (melting temperature of mild steel) which is a minimum for the temperature of the slag in immediate contact with the liquid steel and therefore with an inclusion at the interface slag-metal.

Two parameters have to be considered:

$$\beta = \frac{C_i - C_o}{C_s - \alpha C_i} \tag{6.1}$$

and $$\alpha = v C_s \tag{6.2}$$

C_i is the sphere solution concentration per unit volume of solution. In the present calculation it is determined at 1515°C as the concentration in equilibrium with pure Al_2O_3. It is determined on the binary diagram (Figure 3) as 36 w% or $0.36 \times 2.69 \times 10^3 kg/m^3$ multiplying by the density of the slag.

C_0 is the initial concentration of Al_2O_3 in the slag. In a 70/30 CaF_2/Al_2O_3 slag it is 30 w% or $0.30 \times 2.69 \times 10^{+3} kg/m^3$ of solution

C_s is the concentration of solute in the sphere. Here, considering a pure Al_2O_3 sphere it is the mass density of Al_2O_3 $3.2 \times 10^3 kg\ m^{-3}$

α is the ratio of the volume attributed to a mass of solute in the solution to the volume occupied by the same mass in the pure solute. In this calculation as for the determination of the density of the mixture CaF_2 - Al_2O_3 it is assumed to be unity in the absence of alternative data.

This gives $\beta \approx 0.07$. By interpolation between the curves computed by Readey and Cooper, an estimation can be obtained for the quantity:

$$\frac{Dt}{a_o^2} \sim 7 \qquad (6.3)$$

where D is the coefficient of diffusion

a_o the initial radius of the sphere

t the complete dissolution time.

The value of D determined by the rotating disk experiment for a 70/30 CaF_2/Al_2O_3 slag is used for the estimation of the dissolution time.

For a sphere of initial radius $a_o = 400\mu$ the time necessary for complete dissolution is estimated as $t \sim 130$ sec. For a sphere of 40μ of radius the time for complete dissolution can be estimated as 1.3 sec.

From these assessments, it can be assumed that all inclusions of the size range generally found in steels ($<40\mu$) dissolve readily in contact with the slag. The influence of the temperature of the slag on the dissolution time is important. At 1560°C the time of complete dissolution of a sphere of 400μ can be estimated at 50 seconds and that of a sphere of 40μ of radius at 0.5 seconds. Also, it is to be believed that the stirring of the slag may reduce sharply the dissolution time.

(2) Dissolution, Assuming Similar Flow Conditions to the Rotating Disk System

Assuming that the flow conditions around a particle are similar to those created by the rotating disk, another estimation of the extent of dissolution of the particles can be made. In a 70/30 CaF_2/Al_2O_3 slag at 1518°C the mass flux of Al_2O_3 dissolved per unit time and unit surface area has been determined experimentally for a rotating disk:

$$J = .87 \times 10^{-3} \sqrt{N} \text{ kg m}^{-2} \text{ sec}^{-1} \tag{6.4}$$

Assuming steady state conditions, the rate of dissolution of a sphere is:

$$\frac{d\,(4/3\ \pi r^3 \times C_s)}{dt} = -4\ \pi r^2\ J \tag{6.6}$$

or

$$C_s \frac{dr}{dt} = -J \tag{6.7}$$

The time required to dissolve completely a sphere of initial radius a_o is therefore:

$$t = \frac{a_o\ C_s}{J} \tag{6.8}$$

Let us compare the flow conditions around a rotating disk to those around the tip of the electrode assuming that this is conical.

Reynolds number for a rotating disk is:

$$Re = \frac{\omega R^2}{\nu} \tag{6.9}$$

and for a cone:

$$Re = \frac{UX}{\nu}$$

where U is the flow rate along the sides of the cone and X the length of the cone exposed to the flow. For an electrode of 0.03 m in diameter with a summit angle of 60° and assuming a flow rate of 0.10m sec^{-1}

$$Re \sim 140 \tag{6.11}$$

Taking the same Reynolds number for the rotating disk would give

$$\omega = 30 \text{ rd}$$

or $$N \simeq 300 \text{ r.p.m.}$$

So, assuming that in both cases the thickness of the diffusion boundary layers are the same or of the same order of magnitude, a flow rate of 10 cm sec^{-1} along the sides of a cone at the tip of an electrode of 0.03 m in diameter produces the same dissolution rate as in the case of the rotating disk system at at 300 r.p.m. at 1518°C from (6.4)

$$J = 1.5 \times 10^{-2} \text{ kg m}^{-2} \text{ sec}^{-1}$$

Putting this value into (6.8), the time necessary to dissolve an alumina sphere of 400μ of radius completely would be of the order of 80 seconds. For a sphere of 40μ of radius, this time would be 8 seconds.

It is difficult to estimate how long an inclusion may be in contact with the slag during processing, as the metal flows along the electrode tip to form a droplet, then as this droplet falls through the slag and then at the surface of the liquid metal pool. The droplets fall from the tip of the electrode at intervals of about 1 second. It can be assumed that this is also the time for the droplet to form. In total the time during which an inclusion may react with the slag can be estimated to be of the order of a few seconds. According to the preceding calculations it can be assumed that all particles of radius smaller than 40μ will dissolve readily as they come into contact with the steel.

The range size of the particles introduced artifically in the electrode has been chosen between 400μ and 800μ so that it can be expected that some of these particles will be present in the ingot with an only slightly reduced size.

VII. EXPERIMENTS WITH ARTIFICIALLY INTRODUCED PARTICLES IN THE ELECTRODE

Three different experiments were made with particles ranging from 400μ to 800μ artificially introduced in the electrode. After remelting, samples were taken out of the electrode to be observed with the microprobe. In addition, the solidification conditions which are believed to have an influence on the removal of inclusions were studied.

(1) The Making of the Electrodes

a) alumina particles were introduced in a mild steel electrode of 32 x 10^{-3}m in diameter. The particles were put in holes bored in the electrode at 0.0375 intervals and secured with a bolt.

b) silica particles were introduced in the same way in a mild steel electrode.

c) alumina particles were introduced in a Ferro Vac-E electrode of 25 x 10^{-3}m in diameter. The particles were vacuum hot-pressed with iron powder (previously deoxidized by H_2 gas) in the weight ratio 1/6 of $Al_2)_3$/Fe. The size of the small cylindrical compacts was about 0.01m in diameter and 0.006 m in length. Fourteen were inserted in the electrode at 0.025 m intervals and the hole was closed with a Ferro Vac-E plug.

(2) The Melting Conditions of the Electrodes

The three electrodes were remelted in the Universtiy of British Columbia's electroslag unit. The two mild electrodes were remelted in copper mold of 77 x 10^{-3}m in diameter using a 70/30 CaF_2-CaO/Al_2O_3 slag. The Ferro Vac-E Electrode was remelted in a mold of 58 x 10^{-3}m in diameter, using a 70/30 CaF_2/Al_2O_3 slag. In the three experiments,the polarity of the electrode was negative and that of the ingot positive. The difference of potential between the electrode and the ingot was maintained at about 23 volts. The intensity of the current was about 1000 Amps. 0.3 kg of slag was used, which made a height of 0.04 m of molten slag in the mold. Droplets of about 650μ in diameter formed at intervals of 1 second. In the three cases the average solidification rate was about 10^{-4}m sec^{-1}.

(3) The Remelting of the Mild Steel Electrodes

a) Inclusions in the electrode

The mild steel used was A.I.S.I. C 1018. Its analytical specification is:

C	0.15 - 0.20%
Mn	0.60 - 0.90%
P_{max}	0.040%
S_{max}	0.050%

Samples of this steel were polished and observed with the microprobe to see what types of inclusions were contained in the steel. All inclusions were found to contain Mn. Some of them contained also S or/and Si. So, it can be said that all inclusions are either MnS or MnO inclusions, some of them with a slight concentration of SiO_2. One inclusion was found to contain Ca, but it does not seem typical in that respect. A micrograph of this inclusion is shown on Figure 9. Besides containing Ca (Figure 10), it contains Mn as main element (Figure 11) and a slight concentration of Si (Figure 12). At one end, there is a concentration of sulphur as detected with a S trace (Figure 13). Some of the small rounded inclusions (Figure 9), the size of which is less than 2μ, do not seem to contain Mn; they may be FeO inclusions.

The maximum size of the inclusions observed was 25μ. The total number of inclusions of all sizes can be estimated at 10^{+11} per m^3 of metal.

b) Inclusions in the ingot

The same types of inclusions were found in both ingots after remelting of the electrodes one of which contained Al_2O_3 particles and the other SiO_2 particles. In both ingots, Al was detected in all the inclusions and in addition Mn was detected in some of them. No silicon was detected. Silica dissolves readily in CaF_2 - Al_2O_3 slags as a preliminary experiment using the rotating disk electrode had shown. This was an attempt to calculate the diffusion coefficient of silica

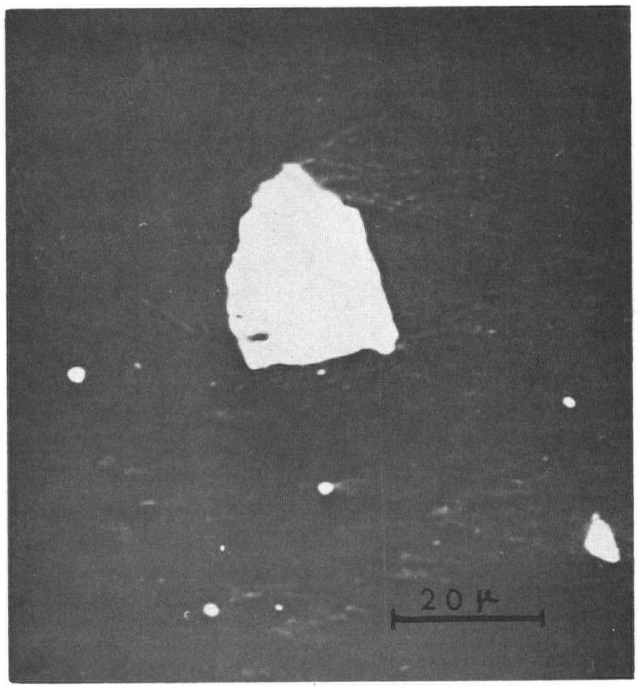

Figure 9 Typical inclusion in the mild steel electrode (X 1200)

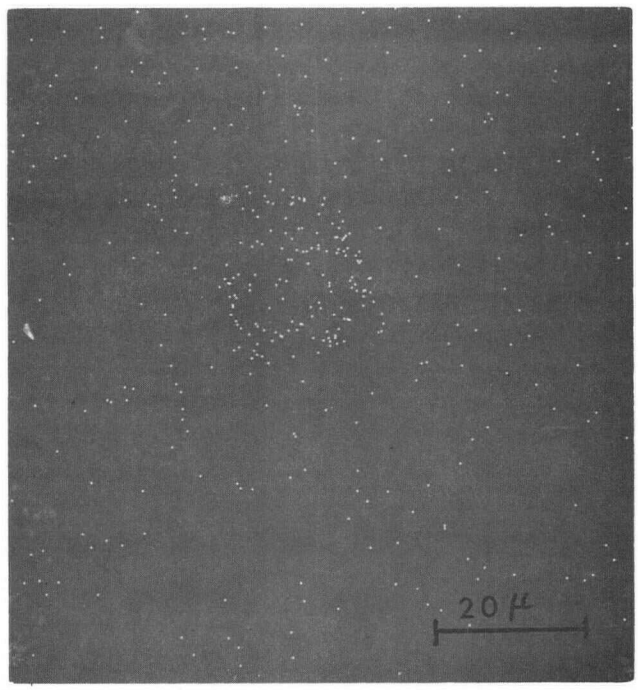

Figure 10 X-Ray picture for Ca (X 1200)

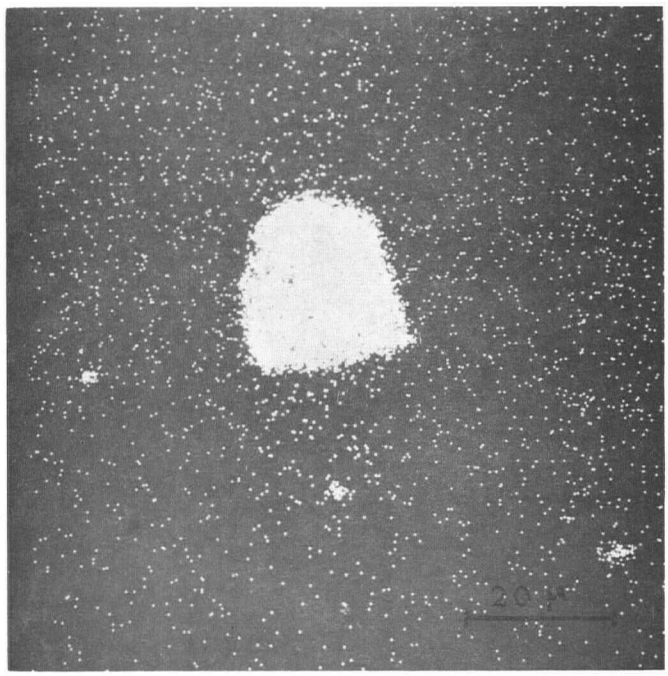

Figure 11 X-Ray picture for Mn (X 1200)

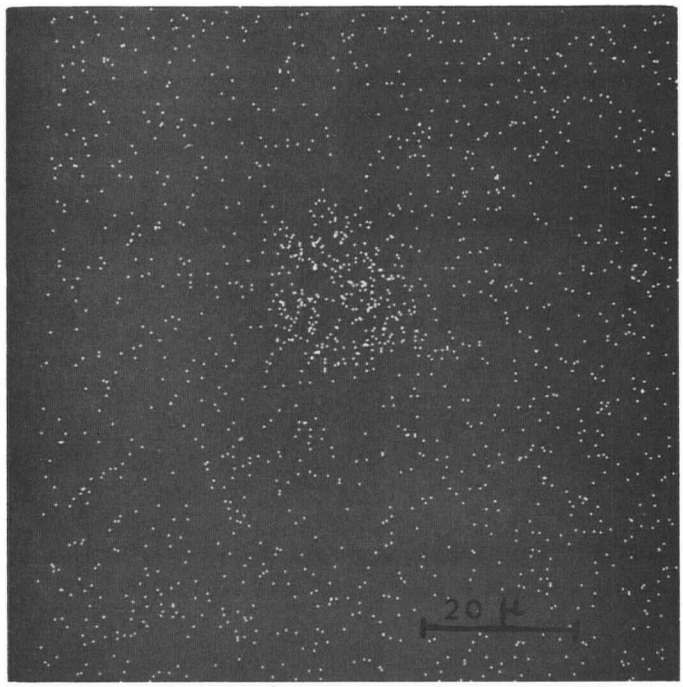

Figure 12 X-Ray picture for Si (X 1200)

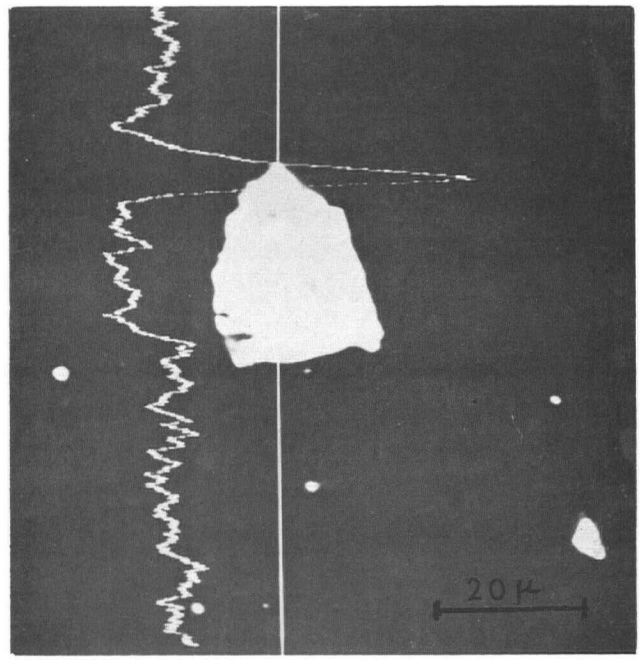

Figure 13 Absorbed electron image plus S trace

in slags in the same way as the diffusion coefficient of alumina had been determined. It is to be believed that silica also dissolves readily in CaF_2 - CaO/Al_2O_3 slags containing no silica. As a consequence, no silica inclusions coming from the particles added artificially could be found. And the silicon that had been detected in the MnS or MnO inclusions of the electrode could not be detected in those of the ingots. No sulfur was detected. This can be explained by the efficiency of the slag metal reaction:

$$[S] + (O^{2-}) = (S^{2-}) + [O] \qquad (7.1)$$

Typical inclusions are shown on Figure 14, their aluminum content detected with the microprobe on Figure 15 and their manganese content on Figure 16. The presence of alumina inclusions in both ingots when alumina particles was added to only one of the electrodes and when the steel of the electrode contained no alumina inclusions is puzzling. It could be explained by an exchange reaction between the MnO or MnS inclusions of the electrode and the Al_2O_3 of the slag. However, some other mechanism can take place which can be investigated by remelting a steel free of all inclusions, for instance Ferro Vac-E.

(4) The Remelting of a Ferro Vac-E Electrode

a) The electrode

Ferro Vac-E is almost pure iron. A typical analysis of Ferro Vac-E is listed below:

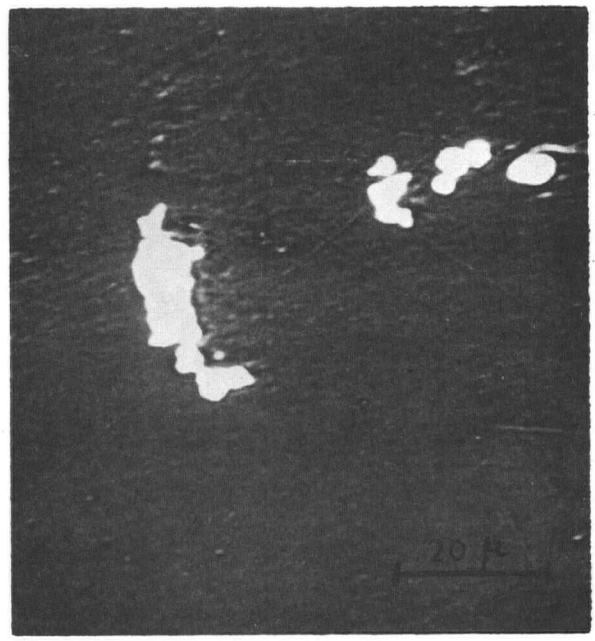

Figure 14 Typical inclusion in the ingot after remelting of the mild steel electrode (X 1200)

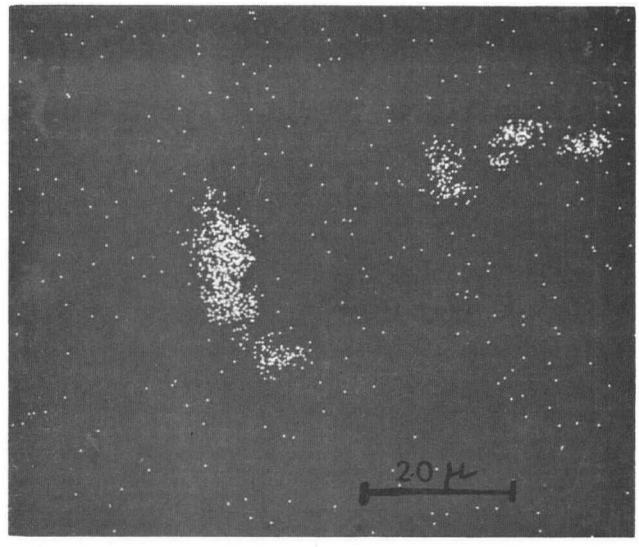

Figure 15 X-Ray picture for Al (X 1200)

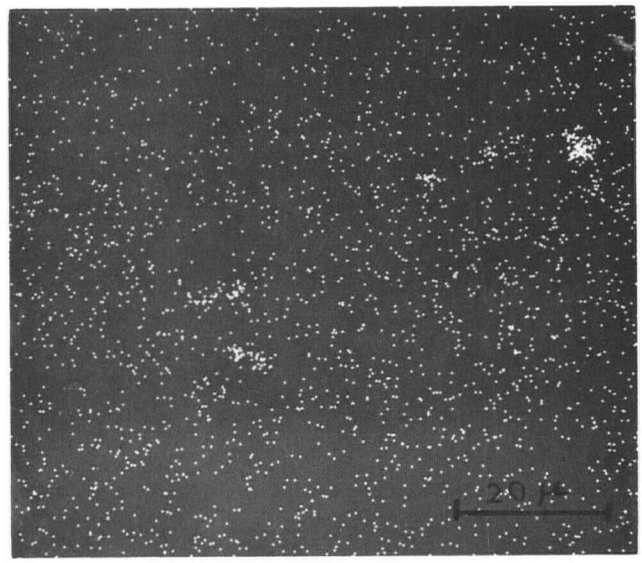

Figure 16 X-Ray picture for Mn (X 1200)

C	.005%
Mn	.0005%
P	.003%
S	.005%
Si	.006%
Ni	.02%
Cr	.006%
V	.004%
W	.01%
Mo	.001%
Cu	.01%
Ce	.006%
N	.00085%
O_2	.0030%
H_2	.000025%

It is free of all inclusions dectectable with the microprobe. The alumina particles were put into the electrode in the form of compacts with iron powder to ensure that upon melting the particles would remain entrapped in the liquid metal.

b) Inclusions in the ingot

Samples of metal taken out of the ingot were polished and observed with the microprobe. The biggest inclusions in the size range 5 - 15μ were all found to contain Al. Some of them have variable concentrations of Fe. The number of these inclusions in the range size 5 - 15μ can be assessed at 10^{+12}

per m^3 of metal. This number is far higher than the number of particles artificially introduced in the electrode (a few hundreds). Even if these particles, the original size of which was in the range 400 - 800μ had dissolved partially down to the size of the biggest inclusions found in the ingot(15μ), they could only account for the presence of only a few of them. Therefore, the presence of the alumina inclusions in the ingot does not depend on the alumina inclusion content of the electrode.

Besides these inclusions, a great number of small rounded inclusions < 3μ could be observed. They are believed to be FeO inclusions. It is difficult to make an iron-count on them because of their very small size. Figure 17 gives a photograph of a cluster of inclusions of all sizes. The Al concentration appears on Figure 18 and the Fe concentration on Figure 19. No calcium was detected; consequently no inclusions are slag inclusions or pieces of skin entrapped in the freezing metal.

The presence of the alumina, iron aluminates and iron oxide inclusions can be explained either by a mechanism of dissolution of the Al_2O_3 particles in the melting iron and then renucleation upon freezing or by an electrochemical mechanism. The remelting of the mild steel electrode which did not contain Al_2O_3 but SiO_2 particles and the remelting of a Ferro Vac-E electrode which did not contain any added particles have given ingots in which the same types of inclusions could be observed. The electrochemical mechanism seems therefore preponderant. In

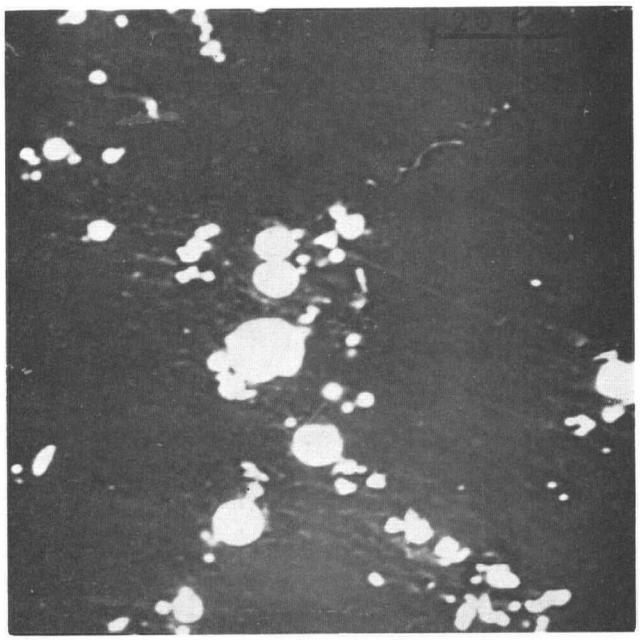

Figure 17 Cluster of inclusions in the ingot after remelting of Ferro Vac-E electrode

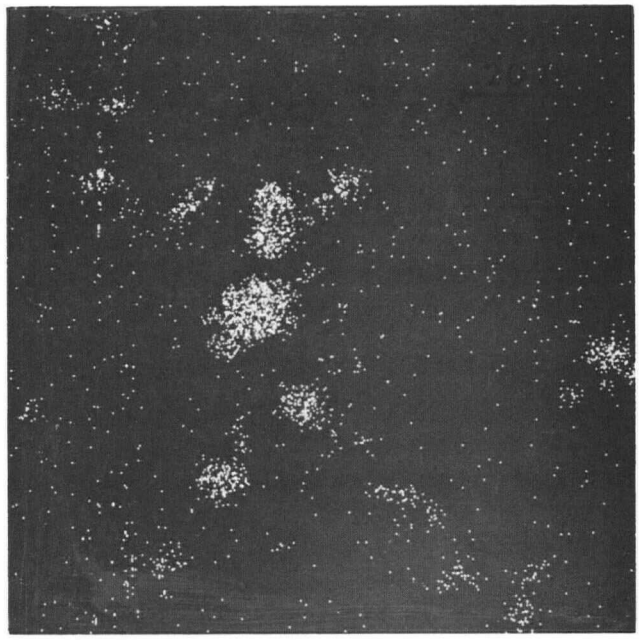

Figure 18 X-Ray picture for Al (X 1200)

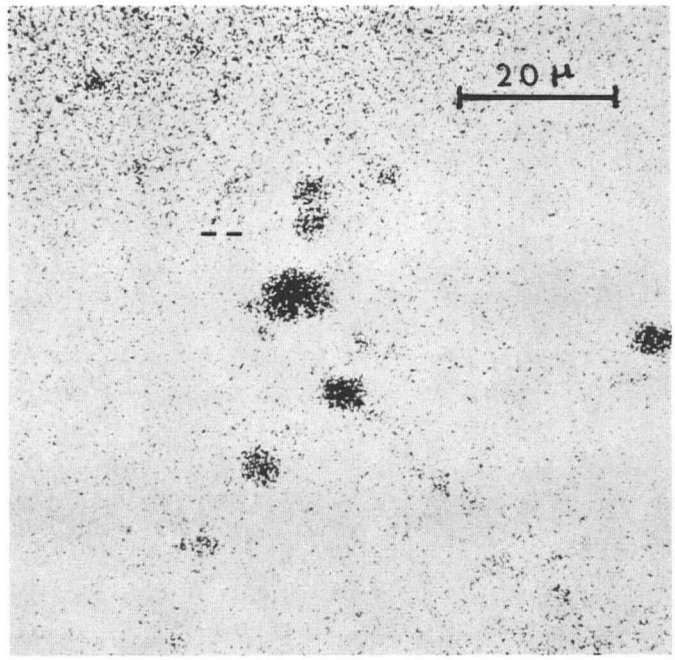

Figure 19 X-Ray picture for Fe (X 1200)

addition, Kay[23] has shown that the quantity of Al_2O_3 that could dissolve in the liquid metal was very small.

(5) Electrochemical Mechanism During Remelting

During refining the electrode is electrically negative and the ingot positive. The slag as ionic solution is composed mainly of the following ionic species:

$$Al^{3+}\ Ca^{++},\ AlO_2^{-},\ O^{2-},\ F^{-}$$

The following reactions can occur at the cathode (electrode)

$$Ca^{2+} + 2\bar{e} = Ca\ (g)\ \text{or}\ (Ca)_{CaF_2} \qquad (7.2)$$

$$Al^{3+} + 3\bar{e} = [Al] \qquad (7.3)$$

and at the anode (ingot):

$$O^{2-} = [O] + 2\bar{e} \qquad (7.4)$$

So there is oxidation of the liquid metal at the ingot anode and electrochemical formation of aluminum at the cathodic electrode. Aluminum and oxygen dissolve in liquid steel. Upon solidification, deoxidation inclusions can nucleate in the ingot and according to the nucleation theory of inclusions presented by Turpin and Elliot[12], Al_2O_3, ion aluminates and iron oxide inclusions can be found in the ingots. Calcium is gaseous at the temperature of liquid steel and is not soluble in steel. Accordingly, no calcium was detected in the inclusions of the ingots.

(6) Remarks on the Solidification of the Ingot

It has been noted in Chapter II that the solidification conditions of the ingot had an influence on the removal of inclusions. The factors to consider are the solidification rate, the concavity of the interface and the interdendirtic spacing.

a) Solidification rate

The average solidification rate has been calculated. The size of the inclusions that would be removed according to Stokes' law has been then determined on the curves plotted on Figure 2. Table 3 gives a summary of these determinations:

TABLE 3

	average solidification velocity	minimum size of inclusions removed
Ferro Vac-E + Al_2O_3 particles	$0.17\ 10^{-3}$m sec^{-1}	8μ
mild steel + Al_2O_3 particles	$0.10\ 10^{-3}$m sec^{-1}	6μ
mild teel + SiO_2 particles	$0.09\ 10^{-3}$m sec^{-1}	6μ

As reported previously, larger inclusions than this are found in the ingot. Convection currents in the liquid metal pool above the ingot perturbed the rising of the particles according to Stokes' law. It does not seem that a simple buoyancy argument can be applied to this case.

b) Concavity of the interface

The surface of a section of the Ferro Vac-E ingot has been polished and etched for 30 seconds with a solution of 2% Nital. Figure 20 gives a photograph of this etched section. The direction of the grains can be observed. The direction of solidification is vertical for the central part of the ingot. At the surface it makes an angle of about 45° with the vertical line. An interface line has been tentatively drawn on the photograph.

c) Interdendirtic spacing

Ferro Vac-E which is almost free of carbon content does not exhibit any dendrites. On an etched section, elongated grains in the direction of solidification can be observed. Mild steel solidifies dendritically. Figure 21 shows a micrograph of the dendrites.

The interdendritic spacings have been measured in the middle region of the ingot of mild steel with Al_2O_3 particles.

The average spacing has been found to be:

$i = 290\ \mu$

$\sigma = 120\ \mu$

They range from 140 μ up to 620 μ.

Weinberg and Buhr[15] have measured the interdendritic spacings as a function of their distance from the chill and they

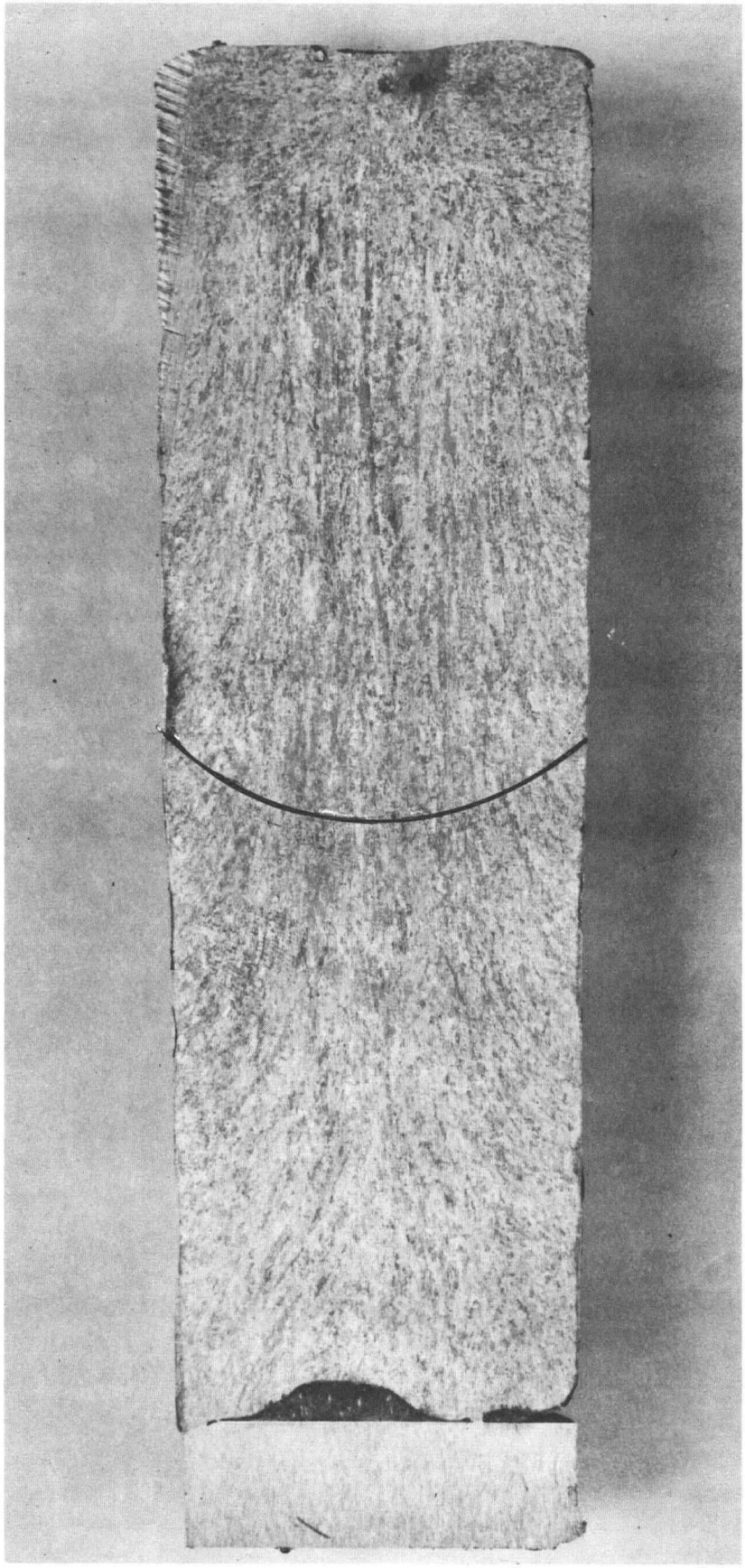

Figure 20 Etched section of the ingot after remelting the Ferro Vac-E electrode

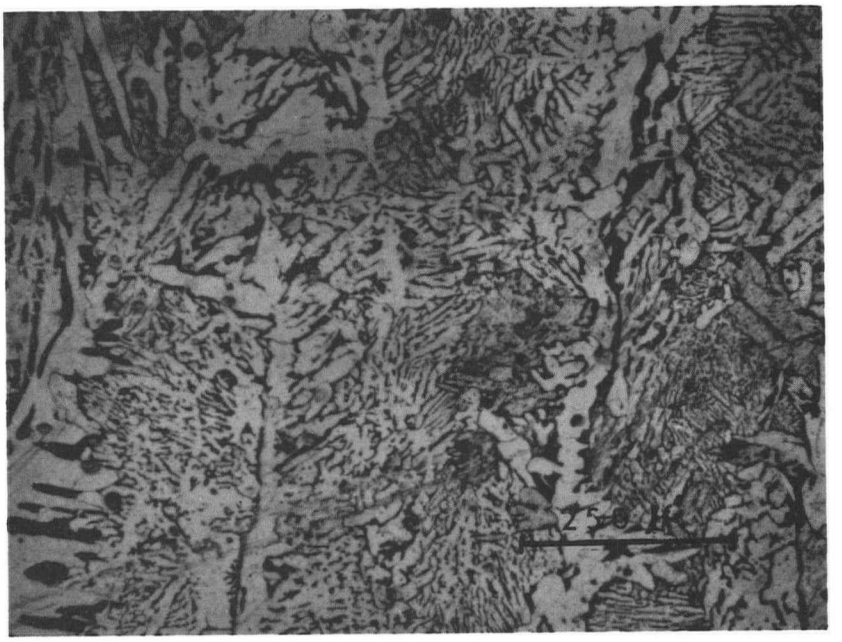

Figure 21 Dendrites on the polished and etched surface of a specimen of the ingot obtained after re-menting a mild steel electrode

have determined the function of the interface position with respect to time for their experiment. The advance of the interface is proportional to the square root of the time. In the experiment with the electroslag the advance of the interface is proportional to time since the solidification velocity is held constant. From Weinberg's and Buhr's results it is possible to calculate the function of the interdendritic spacing with respect to the solidification velocity. The details of the calculations are given in Appendix V. The relation is found to be:

$$i = \frac{50 \times 10^{+3}}{V}$$

i interdendritic spacing in μ

V solidification velocity in μ sec^{-1}

The interdendritic measurements were made on the section of the mild steel with Al_2O_3 particles ingot. Its average solidification velocity is 0.10 10^{-3} sec^{-1}. According to the relation derived from Weinberg's and Buhr's measurements this would give

$$i = 500\ \mu$$

This average value is greater than the value of 290 μ which was measured, although it falls in the upper bracket of 290 ± σ (σ = 120 μ). The value that has been measured in the present experiment would correspond to a melting rate of 0.17 10^{-3}m/sec. Of course, during remelting there are variations in the solidification velocity around the average value. It is controlled

by the feeding rate of the electrode. There are, however, no variations of 70% in the feeding rate of the electrode. The purpose in measuring of the interdendritic spacing for this study is to explain the phenomenon of entrapment. The interdentritic spacing is one order of magnitude higher than the average size of the biggest inclusions in ordinary steels. It seems that the inclusion sees the interface and the dendrites as smooth and, if there is entrapment, it is more likely to happen between the secondary dendrites, the spacing of which is much smaller as observed by Weinberg and Buhr.[15] Also the interdendritic spacing indicates the spacing of the projections ahead of the interface, but it does not say how far these project ahead of the interface. It is to be believed that it is of the order of magnitude of the secondary interdentritic spacings which are two or three times smaller than the corresponding primary dendritic spacings. From the point of view of an inclusion, the interface appears therefore flat and smooth, and it seems that inclusions are rather pushed ahead than entrapped.

CONCLUSIONS

Different mechanisms can account for the behaviour of inclusions during electroslag remelting. They are controlled by the composition of the slag and the solidification conditions of the ingot.

Inclusions can dissolve partially or totally in the liquid metal and then renucleate as the metal solidifies. This phenomenon has not been observed in the experiment with added particles of silica in the electrode and it does not account for the presence of the alumina inclusions in the ingots, as predicted by Kay's calculations.[23]

Inclusions can dissolve readily in contact with the slag, such as silica inclusions in 70/30 CaF_2/Al_2O_3 slags. From the value of the diffusion coefficient and from dissolution calculations it was thought that big particles (800 μ) artificially introduced in the electrode would not dissolve completely. This is not the case and it is found that even big alumina particles dissolve very rapidly because of high temperature and strong convection currents.

The presence of the large number of inclusions in the ingots can only be explained by an electrochemical mechanism. Electrolytic oxidation and electrolytic dissolution of aluminum on the electrodes takes place in 70/30 CaF_2/Al_2O_3 slags.

Then alumina, iron aluminates and iron oxide inclusions nucleate during freezing. The electrolytic phenomenon, which had not been observed before without ambiguity, is controlled by the current density delivered by the electrodes to the slag, and by the ionic composition of this slag. These dependence relationships deserve further study.

Most inclusions are found to be very small ($< 4\mu$), but a large number of inclusions are in the size range 10 to 15 μ. From Stokes' law inclusions over 8 μ should be removed, but a simple buoyancy mechanism cannot account for the floating of inclusions in the stirred metal pool above the ingot. The entrapment of inclusions between dendrites does not seem to be a significant mechanism in view of the small size of the inclusions relative to the interdendritic spacing.

No droplets of slag or pieces of slag skin entrapped in the solidifying ingot could be observed in the ingots.

SUGGESTIONS FOR FUTURE WORK

(1) The mechanism of dissolution of inclusions has been studied in the simple case of alumina inclusions dissolving in CaF_2 - Al_2O_3 slags in which the diffusion coefficient of alumina is relatively high. Other slag compositions should be investigated. For instance, the diffusion coefficients of alumina in molten oxide mixtures, determined by Shurygin and Boronenkov,[29] are one order of magnitude smaller than the value determined in this study in CaF_2 - Al_2O_3 slags.

(2) The dissolution of silica should be investigated more closely, particularily in high silica concentration slags. It should also be determined whether or not electroprecipitation of silicon occurs on the cathode.

(3) The influence of the current density on the electrolytic dissolution of aluminum should be investigated. In particular, industrial process units work with a smaller current density than the University of British Columbia unit.

(4) The influence of the ionic composition of the slag with respect to the solubility in liquid metal of the different elements which could form on the electrodes should be investigated. For instance, Ca^{2+} ions give rise to Ca, which does not dissolve in liquid metal and, therefore, is not found in the inclusions.

(5) The melting parameters of the electrode control the solidification rate and the shape of the molten metal pool. Their influence on the removal of inclusions by floatation in the liquid metal pool should be investigated.

(6) Another question is whether or not there is significant electromagnetic stirring of the slag and of the liquid metal pool, and what is its influence on the removal of inclusions.

REFERENCES

1. Kiessling, R. "Non metallic inclusions in steel." Part III, I.S.I. Publication 115,(1968).

2. Atkinson, M. J.I.S.I. 195, 64,(1960).

3. Duckworth, W.E. and Ineson. I.S.I. Special report 77, p. 87,(1963).

4. Allmand, T.R. J.I.S.I. 190, 359,(1959).

5. Kiessling, R. "Non metallic inclusions in steel." Parts I and II, I.S.I. publications 90 and 100,(1964-66).

6. Snow, R.B. J. Of Metals. (October 1968),55.

7. Smerko, R.G. and Flinchbaugh, D.A. J. of Metals,(July 1968), 43.

8. Segawa, K. Trans. I.S.I.J. 7, 163,(1967).

9. Miyashita, Y. and Nishikawa, K. Trans. I.S.I.J. 8, 181, (1968).

10. Torrsell, K, Jernkontoret, Ann. 151, 12,(1967).

11. Turkdogan, E.T. J.I.S.I. (September 1966) 914.

12. Turpin, M.L. and Elliott, J.F. J.I.S.I. (March 1966),217.

13. Torsell, K., Gatellier, C., Olette, M., C.R. Acad. Sc., Paris, t 267, serie C, 869,(1968).

14. Turkdogan, E.T. Trans. A.I.M.E. 233, 2100,(1965).

15. Weinberg, F. and Buhr, R.K. "The solidification of metals." I.S.I., p. 110.

16. Medovon, B.I. Latash, Yu.V., Maksimovich, B.I., and Stupark, L.M. "Electroslag remelting." State Scientific and Technical Publishing House of Literature on Ferrous and Non-Ferrous Metallurgy, Moscow,(1963).

17. Antoine, L., Boucher, A., Guibert, G. and Jallas, P. Revue de metallurgie, 7-8, 623,(1967).

18. Prianichkov, I.S., Topiline, V.V., Kliouev, M.M. and Medovar, B.I. Revue de metallurgie, 99, 649,(1967).

19. Bhat, G.K. Proc. Intern. Symp. on electroslag remelting, Mellon Institute, 1967, Part I, paper 1.

20. Mitchell and Etienne M. Trans A.I.M.E., 242, 1462, (1968).

21. Salt, D.J. Proc. Intern. Symp. on electroslag remelting. Mellon Institute, 1967, Part I, Paper 2.

22. Holzgruber, W. Proc. Intern. Symposium on electroslag remelting. Mellon Institute, 1967, Part II, Paper 3.

23. Kay, D.A.R. Proc. Intern. Symp. on electroslag remelting. Mellon Institute, 1967, Part II, Paper 4.

24. Mitchell, A. Proc. Intern. Symp. on electroslag remelting. Mellon Institute, 1967, Part II, Paper 5.

25. Bockris, J. "Modern aspects of electrochemistry." Part II, London, (1959).

26. "Molten salt chemistry." edited by Blander, Interscience Publishers,(1964).

27. Borucka, A.Z., Bockris, J. and Kitchener, J. J. of chemical physics, 24, 1282, (1956).

28. Towers, H. and Chipman, J. Trans A.I.M.E., 209, 769, (1957).

29. Shurygin, P.M. and Boronenkov, V.N. Liteinoe Proizv, (1963), No. 8, p. 22.

30. Shurygin, P.M., Boronenkov, V.N. and Kryuk, V.I. Sb.Nauchn. Tr., Ural'sk. Politekhn. Inst., 126, 80, (1963).

31. Shurygin, P.M., Barmin, L.I. and Esin, O.A. Chernaya Metallurgia 5, (12), 5 (1962).

32. Levich, V.G. "Physicochemical hydrodynamics." Prentice-Hall, (1962).

33. Kassner, J.F. J. electroch. Soc., 114, 689, (1967).

34. Olsson, R.G., Perzak, T.F., Koump, V. Trans. A.I.M.E., 242, 776, (1968).

35. Riddiford, A.C. in "Advances in electrochemistry and electrochemical engineering." Vol. 4, edited by Delahay and Tobias,(1966).

36. Darken, L.S. and Gurry, R.W. "Physical chemistry of metals." McGraw-Hill, New York, (1953).

37. Muan, A., Osborn, E.F. "Phase equilibria among oxides in steelmaking." sponsored by A.I.S.I., (1965).

38. Glassner, A. "The Thermochemical properties of the oxides, fluorides and chlorides to 2500°K." Argonne National Laboratory, U.S. Atomic Energy Commission, (1957).

39. Shulz, D.A. and Searcey, A.W. J. Phys. Chem. 67, 103, (1963).

40. Kuo Chu-Kun and Yen Tung-Sheng. Acta Chim. Sinica 30, 381, (1964).

41. Buist, D.S. Mineralogical magazine, 36, 281, 676, (1968).

42. Janz, G.J. "Molten salts handbook." Academic Press, (1967).

43. Joshi, S., Mitchell,A. unpublished research.

44. Kirshenbaum, A.D., Cahill, J.A. and Stokes, C.S. Inorg. Nucl. Chem. 5, 297, (1960).

45. Evseev, P.P. Avtom Svarka n° 11, (176), 42, (1967).

46. Kammel, V.R. and Winterhagen, H. Erzmetall, 21, 399, (1968).

47. Readey, D.W., Cooper, Jr. A.R. "Molecular diffusion with a moving boundary and spherical symmetry." M.I.T. Private communication.

APPENDIX I

X-Ray powder diffraction results -

60/40 CaF_2/Al_2O_3

d spacing	intensity	identified as
3.52	s	Al_2O_3
3.14	vs	CaF_2
2.56	vw	Al_2O_3
2.38	vvw	Al_2O_3
2.33	vvw	unidentified
2.12	vw	unidentified
2.08	vw	Al_2O_3
2.02	w	unidentified
1.92	vvs	CaF_2
1.81	vvw	unidentified
1.74	vvw	Al_2O_3
1.64	s	CaF_2
1.59	s	Al_2O_3
1.40	vw	Al_2O_3
1.36	w	CaF_2
1.25	w	CaF_2
1.23	w	CaF_2
1.11	s	CaF_2
1.05	vvw	CaF_2
0.995	vvw	unidentified
0.964	vvw	CaF_2
0.921	vw	CaF_2

Key:				
	vvs	very, very strong	w	weak
	vs	very strong	vw	very weak
	s	strong	vvw	very, very weak

APPENDIX II

Experimental data

Dissolution of alumina disks in a 70/30 CaF_2/Al_2O_3 slag at 1518°C

Rotating speed r.p.m.	dissolution time sec	weight loss x 10^{+6} kg sec^{-1}
50	64.8	2.9
50	33.3	3.8
50	36.8	2.0
100	42.0	3.5
100	42.1	4.6
100	44.2	3.9
100	39.4	7.2
100	27.8	6.9
145	26.1	8.6
145	44.0	6.3
170	44.3	5.6
200	39.9	6.0
200	33.8	9.3
200	37.8	7.8
200	43.5	7.2
225	41.0	7.8
255	30.3	8.8
300	28.4	11.3
300	24.3	9.6
400	31.2	10.7
400	23.2	11.8
400	27.3	10.5

APPENDIX III

Experimental data

Dissolution of alumina disks in a 70/30 CaF_2/Al_2O_3 slag at 1509°C

rotating speed r.p.m.	dissolution time sec	weight loss x 10^{+6} kg sec^{-1}
100	37.4	3.0
100	36.9	5.2
100	27.6	3.0
100	39.4	3.2
120	27.0	6.9
145	37.7	5.6
145	41.3	5.3
200	43.9	4.7
300	35.1	7.4
300	26.9	7.1
400	30.1	7.8

APPENDIX IV

Experimental data

Dissolution of alumina disks in a 80/20 CaF_2/Al_2O_3 slag at 1500°C

rotating speed r.p.m	dissolution time sec	weight loss 10^{+6} kg sec^{-1}
100	29.3	6.9
100	32.3	7.0
145	31.9	7.6
200	36.4	7.8
225	36.2	8.9
300	30.4	9.8
350	26.2	12.6
400	24.3	13.3

APPENDIX V

Calculation of the Interdendritic Spacing as a Function of the Solidification Velocity, Using Weinberg's and Buhr's Results[15]

The position of the interface as a function of $t^{1/2}$ is expressed by the relation:

$$Y = 1.20 \sqrt{t} - 0.35 \qquad (1)$$

Y is expressed in inches and t in minutes. Expressing Y in μ and t in seconds, it follows:

$$Y = 25000 \left(1.20 \sqrt{\frac{t}{60}} - .35\right)$$

or

$$Y = 3870 \sqrt{t} - 8750 \qquad (2)$$

The solidification velocity is:

$$Y = \frac{dY}{dt} = \frac{1940}{\sqrt{t}} \ \mu \ \sec^{-1} \qquad (3)$$

From Figure 4 of the paper, the dendritic spacing can be expressed as a function of Y. $Y < 10^5$. The equation is:

$$i = 6700 \ Y + 60 \qquad (4)$$

i interdendritic spacing in μ

Y can be eliminated between equations (2) and (4). It follows:

$$i = 26 \sqrt{t} \qquad (5)$$

$\sqrt{t}$ can be eliminated between (5) and (3). i is obtained as a function of the solidification velocity v:

$$i = \frac{50 \times 10^3}{v} \qquad (6)$$

i interdendritic spacing in μ

v solidification velocity in μ sec^{-1}